Latin American Journal of Solids and Structures
www.lajss.org

A Model for Homogenization of Linear Viscoelastic Periodic Composite Materials with Imperfect Interface

Abstract

In this paper, a micromechanical extension of the finite-volume direct averaging micromechanics theory (FVDAM) is presented for evaluation of the homogenized relaxation moduli of linear viscoelastic unidirectional fiber reinforced composites with periodic microstructures. Such materials are assumed as composed of repeating unit cell with arbitrary internal architectural arrangements of fibers coated by thin flexible interphases. These interphases are replaced by equivalent imperfect interface elements with imposed continuity in tractions and discontinuity in displacements. Indeed, the proposed computational procedure allows an easy and efficient treatment of the displacement discontinuity condition across the interfaces. The viscoelastic behavior of the constituent phases is modeled using the generalized Maxwell model. The formulation is particularly derived for the range of small strains, operating directly in the time domain using a numerical incremental time-stepping procedure based on the concept of internal stress variables. The performance of the proposed approach is demonstrated through homogenization of viscoelastic fiber reinforced composites and periodic multilayer materials with flat and wavy architectures.

Keywords

Homogenization, Viscoelasticity, Imperfect Interface, Finite-Volume Theory.

Romildo dos Santos Escarpini Filho [a]
Severino Pereira Cavalcanti Marques [b]

[a] Campus do Sertão, Federal University of Alagoas, Delmiro Gouveia, 57480-000 Alagoas, Brazil
E-mail: romildo@lccv.ufal.br
[b] Center of Technology, Federal University of Alagoas, Maceió, 57072-900 Alagoas, Brazil
E-mail: smarques@ctec.ufal.br; Tel.: +55 82 3214 1297

http://dx.doi.org/10.1590/1679-78252749

Received 01.01.2016
In revised form 19.07.2016
Accepted 05.08.2016
Available online 29.08.2016

1 INTRODUCTION

The number and variety of engineering applications of fiber reinforced composite materials have greatly increased in recent decades. To assure the continuity of this rapid widespread use, it is essential to have a more complete understanding about the composite material behaviors at different scales. Among the available tools for contributing to this better understanding, the micromechanical theories occupy an important place. Micromechanical modeling provides crucial information on the

relationships between the macroscopic structural behavior of composite materials and the local properties of the constituent phases and their microstructural arrangement. Then, it contributes to the development of new engineered composite materials with desired effective or homogenized properties, identifying the more appropriate constituent phases and microstructural details, based on a multiscale theoretical framework (Cavalcante et al., 2012). Furthermore, for the level of structural components, the micromechanics theory contributes by providing the essential material homogenized properties required by the conventional procedures of macroscopic structural analysis.

A review of the literature shows a large number of analytical and numerical micromechanical models proposed for estimating the homogenized mechanical behavior of composites with random and periodic microstructures (Nemat-Nasser and Mori, 1999, Zaoui, 2002, Cavalcante et al., 2012). However, most of these models are applicable to linear elastic two-phase composites. Homogenization models for nonlinear multiphase composites are less developed and currently have been a subject of significant research (Doghri and Tinel, 2005, Khatam and Pindera, 2009, Cavalcante et al., 2011).

The first contributions to the homogenization of viscoelastic composites were given by Hashin (1965, 1970a,b) and Christensen (1969). They used the well-known composite spheres assemblage model (Hashin, 1962), developed for linear elastic materials, together with the correspondence principle between linear elastic and viscoelastic behaviors to predict the effective moduli of two-phase linear viscoelastic composites. For these viscoelastic composites exhibiting random microstructures, many proposed homogenization approaches consist of extensions of the analytical classical mean-field models based on the Eshelby ellipsoidal inclusion theory (Eshelby, 1957), making use of that correspondence principle (Laws and Mc Laughlin, 1978, Wang and Weng, 1992, Brinson and Lin, 1998, Friebel et al., 2006). On the other hand, for the case of periodic microstructures, the homogenization viscoelastic problem is, in general, solved by using the concept of repeating unit cell with periodic boundary conditions (Luciano and Barbero, 1995, Cavalcante and Marques, 2014). The analytical homogenization models for this last class of composites are restricted to repeating unit cell with particular geometrical shape and very simple internal architectural arrangements. Then, for more elaborated microstructure the use of numerical procedures is needed for accurate predictions of the effective viscoelastic moduli. In these latter modeling studies, the finite-element method is, typically, the more employed numerical technique.

An attractive alternative to the finite-element method in the solution of periodic repeating unit cell (RUC) problems is the parametric finite-volume theory developedby Cavalcante et al. (2007) having as basis the original version constructed by Bansal and Pindera (2003). In that parametric version, the heterogeneous material microstructure is discretized using quadrilateral subvolumes which are mapped into corresponding reference square subvolumes. This mapping has been incorporated into the standard finite-volume direct averaging micromechanics (FVDAM) model and applied successfully to solve several thermal and mechanical homogenization problems (Gattu et al., 2008, Katham and Pindera, 2009, Cavalcante et al., 2011, Cavalcante and Marques, 2014, Escarpini Filho and Marques, 2014). To improve some local interfacial conformability shortcomings between adjacent subvolumes exhibited by the structural version of the parametric finite-volume theory, Cavalcante and Pindera (2012) constructed a higher order formulation on rectangular subdomains named generalized finite-volume theory. Subsequently, this formulation was incorporated into the

FVDAM framework and applied to linear elastic periodic materials undergoing finite deformations (Cavalcante and Pindera, 2014a). The results show that the different orders of the FVDAM theory are very capable of reproducing the homogenized response with good accuracy (Cavalcante and Pindera, 2014b). This issue can also be seen in Cavalcante and Marques (2014) for the viscoelastic macroscopic response in infinitesimal deformation domain. Then, the higher computational cost required by the generalized FVDAM justifies the use of the lower order FVDAM version for the evaluation of the homogenized response.

In this paper a novel micromechanical extension of the FVDAM theory is presented for evaluation of the homogenized relaxation moduli of linear viscoelastic unidirectional fiber reinforced composites with periodic microstructures including the concept of imperfect interfaces. Such materials are assumed as composed of repeating unit cell with arbitrary internal architectural arrangements of fibers coated by thin flexible interphases. These interphases are replaced by equivalent imperfect interfaces with imposed continuity in tractions and discontinuity in displacements (Hashin, 1990, Hashin, 1991, Matzenmiller and Gerlach, 2004, Benveniste, 2006). The strategy consist of determining the effective response of a true three-phase (matrix, interphase and fiber) composite material solving a homogenization problem for a two-phase (matrix and fiber) equivalent composite. To address this issue a new imperfect interface element has been derived and incorporated into the FVDAM framework. It is worth mentioning that, for the first time, an imperfect interface element has been formulated with basis on the finite-volume theory for mechanical analysis of composite material. So, the present formulation corresponds to the first version of the FVDAM theory employing the concept of imperfect interfaces for homogenization of fiber reinforced periodic viscoelastic composites with thin interphases located between the matrix and the fibers.

Indeed, the proposed computational procedure allows an easy and efficient treatment of the displacement discontinuity condition across the interfaces. This can be justified by the fact that in the FVDAM theory the displacement compatibility conditions are imposed in terms of subvolume surface-averaged interfacial values, differently from the classical finite element method that employs compatibility of nodal displacements of adjacent elements. The viscoelastic behavior of the constituent phases (matrix, fibers and interphases) is modeled using the generalized Maxwell model (Marques and Creus, 2012). The formulation is particularly derived for the range of small strains, operating directly in the time domain using a numerical incremental time-stepping procedure based on the concept of internal stress variables (Simo and Hughes, 1998, Tran et al., 2011). All the homogenized components of the relaxation tensor are numerically evaluated at different time steps and their discrete values stored along the analysis for generation of the corresponding relaxation curves through the use of appropriate interpolation functions.Although the presented formulation has been derived for small displacements, it can be readily extended to the case of large rotations with small strains, as briefly explained in Subsection 3.8.

The paper is organized as follows. The local three dimensional viscoelastic formulation used for the individual phases are presented in Section 2. All the numerical procedures used by the homogenization viscoelastic model are described in Section 3. The basic ideas of the FVDAM are briefly presented, followed by the detailed description of the formulation proposed for viscoelastic homogenization. The methodology used to model the imperfect interface element is also derived in Section 3. Finally, numerical examples of viscoelastic homogenization are presented in Section 4. These ex-

amples include viscoelastic fiber reinforced composites and multilayer materials with flat and wavy architectures. Comparisons with analytical solutions show the good performance of the homogenization approach.

NOMENCLATURE

A strain concentration tensor component
C relaxation function
D viscoelastic interface function
E Young's modulus
G shear modulus
H auxiliary time-dependent function
K bulk moduli of the viscoelastic model
N number of branches of the viscoelastic model
L length of the subvolume face
U coefficient of the polynomial approximation

$\boldsymbol{C}$ matrix dependent on the phase properties and time interval
$\boldsymbol{D}$ matrix of subvolume face unit normal vectors
$\boldsymbol{G}$ vector of surface-averaged viscoelastic strain contributions
$\mathbf{H}$ time-dependent function
$\hat{\boldsymbol{J}}$ inverse of the volume-averaged Jacobian
$\boldsymbol{K}$ stiffness matrix
$\boldsymbol{N}$ vector of subvolume face unit normal vectors
$\boldsymbol{U}$ vector of polynomial approximation coefficients
$\widehat{\boldsymbol{U}}'$ global surface-averaged fluctuation displacement vector

h interphase thickness
n unit vector component
q internal stress variables
t time, traction component
u displacement component
u' fluctuating displacement component
v volume fraction
x Cartesian global coordinate
y Cartesian local coordinate

$\mathbf{e}$ deviatoric strain tensor
$\mathbf{q}$ deviatoric internal stress variables
$\mathbf{s}$ deviatoric stress tensor
$\hat{\mathbf{t}}$ surface-averaged traction vector
$\widehat{\mathbf{u}}'$ surface-averaged fluctuation displacement vector

Ω unit cell volume
$\Delta\mathbf{C}$ matrix of differences in the material stiffness matrices
Δt time interval
γ viscoelastic relative parameter
ε strain component
$\hat{\varepsilon}$ surface-averaged strain
$\bar{\varepsilon}$ macroscopic strain
η viscosity constant, parametric coordinate
μ shear moduli of the viscoelastic model
ν Poisson ratio
ξ parametric coordinate
σ stress component
$\hat{\sigma}$ surface-averaged stress
τ relaxation time

$\mathbb{C}$ fourth-order elastic constitutive tensor
$\mathbb{M}$, $\mathbb{P}$,$\mathbb{R}$ fourth-order tensors

Subscripts and superscripts
I interphase, interface
f subvolume face number, fiber
o hydrostatic quantity
p subvolume vertex number
q subvolume number
t time
K bulk
G global
μ shear
∞ elastic branch of the viscoelastic material model
in in-plane
out out-of-plane
$+$ side adjacent to the matrix
$-$ side adjacent to the fiber
$*$ effective quantity

2 LOCAL LINEAR VISCOELASTIC FORMULATION

The composite materials considered in this paper are composed in general of linear viscoelastic isotropic phases consisting of a matrix embedding unidirectional long fibers coated with thin interphases. The fibers and interphases have a periodic spatial arrangement inside the matrix so that the composite material can be assumed as constructed by replicated fundamental building blocks, called repeating unit cells (RUCs), as shown in Fig. 1. It is assumed that the viscoelastic behavior of the

constituent materials is governed by a generalized Maxwell model with an arbitrary number n of branches.

In the three-dimensional isotropic material viscoelastic analysis, the stress and strain states are usually decomposed into their hydrostatic and deviatoric parts. The constitutive relation for the hydrostatic state can be written as

$$\sigma^o(t) = C_K(t)\varepsilon^o(0) + \int_0^t C_K(t-s)\frac{d\varepsilon^o(s)}{ds}ds \tag{1}$$

where σ^o and ε^o are the hydrostatic stress and strain, respectively, and $C_K(t)$ denotes the bulk relaxation function. For the deviatoric state, the relation between the deviatoric stress $(\mathbf{s})$ and strain $(\mathbf{e})$ tensors is given by

$$\mathbf{s}(t) = C_\mu(t)\mathbf{e}(0) + \int_0^t C_\mu(t-s)\frac{d\mathbf{e}(s)}{ds}ds \tag{2}$$

being $C_\mu(t)$ the shear relaxation function.

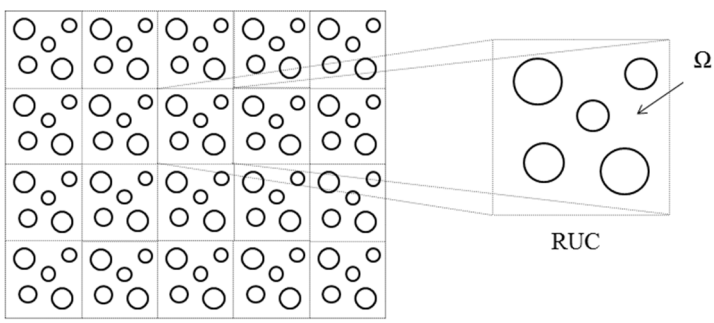

Figure 1: Periodic composite material and repeated unit cell (RUC).

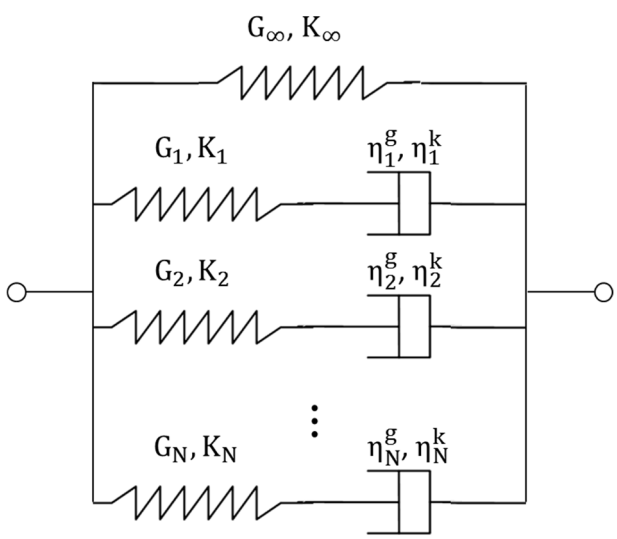

Figure 2: Generalized Maxwell model.

For the generalized Maxwell model with $N+1$ branches (Fig. 2), the bulk and shear relaxation functions are defined by

$$\begin{aligned} \mathrm{C_K}(t) &= 3K_\infty + \sum_{i=1}^{N} 3K_i \exp(-\mathrm{t}/\tau_i^K) \\ \mathrm{C_\mu}(t) &= 2\mu_\infty + \sum_{i=1}^{N} 2\mu_i \exp\left(-\mathrm{t}/\tau_i^\mu\right) \end{aligned} \tag{3}$$

where K_∞ and μ_∞ denote the bulk and shear moduli of the elastic element while K_i and μ_i represent the bulk and shear moduli of the viscoelastic elements that compose the rheological model. τ_i^K and τ_i^μ are the relaxation times related to the hydrostatic and deviatoric viscoelastic behaviors, respectively.

Introducing (3) in (1) and (2), the following expressions are obtained (Marques and Creus, 2012):

$$\sigma^o(t) = \sigma_\infty^o(t) + \sum_{i=1}^{N} \gamma_i^K \, exp(-t/\tau_i^K)\sigma_\infty^o(0) + \sum_{i=1}^{N} q_i^K(t) \tag{4}$$

$$\mathbf{s}(t) = \mathbf{s}_\infty(t) + \sum_{i=1}^{N} \gamma_i^\mu \, exp\left(-t/\tau_i^\mu\right)\mathbf{s}_\infty(0) + \sum_{i=1}^{N} \mathbf{q}_i^\mu(t) \tag{5}$$

where $q_i^K(t)$ and $\boldsymbol{q}_i^\mu(t)$ denote internal stress variables given by

$$q_i^K(t) = \int_0^t \gamma_i^K exp\left(-\frac{t-s}{\tau_i^K}\right)\frac{d\sigma_\infty^o(s)}{ds}ds \tag{6}$$

$$\mathbf{q}_i^\mu(t) = \int_0^t \gamma_i^\mu exp\left(-\frac{t-s}{\tau_i^\mu}\right)\frac{d\mathbf{s}_\infty(s)}{ds}ds \tag{7}$$

being $\sigma_\infty^o(t) = 3K_\infty\varepsilon^o(t)$, $\mathbf{s}_\infty(t) = 2\mu_\infty\mathbf{e}(t)$,$\gamma_i^K = K_i \,/\, K_\infty$ and $\gamma_i^\mu = \mu_i \,/\, \mu_\infty$. These internal stress variables are employed strategically in the incremental time-stepping procedure for the numerical solution of the viscoelastic problem as illustrated below.

At time $t+\Delta t$, equations (6) and (7) can be written in the forms

$$q_i^K(t+\Delta t) = q_i^K(t)exp\left(-\frac{\Delta t}{\tau_i^K}\right) + \gamma_i^K exp\left(-\frac{\Delta t}{\tau_i^K}\right)\int_t^{t+\Delta t} exp\left(-\frac{t-s}{\tau_i}\right)\frac{d\sigma_\infty^o(s)}{ds}ds \tag{8}$$

$$\boldsymbol{q}_i^\mu(t+\Delta t) = \boldsymbol{q}_i^\mu(t)exp\left(-\frac{\Delta t}{\tau_i^\mu}\right) + \gamma_i^\mu exp\left(-\frac{\Delta t}{\tau_i^\mu}\right)\int_t^{t+\Delta t} exp\left(-\frac{t-s}{\tau_i}\right)\frac{d\mathbf{s}_\infty(s)}{ds}ds \tag{9}$$

Using the following approximations for sufficiently small time step Δt,

$$\frac{d\sigma_\infty^o(s)}{ds} \cong \frac{\Delta\sigma_\infty^o}{\Delta t} = \frac{\sigma_\infty^o(t+\Delta t) - \sigma_\infty^o(t)}{\Delta t} \quad \text{e} \quad \frac{d\mathbf{s}_\infty(s)}{ds} \cong \frac{\Delta\mathbf{s}_\infty}{\Delta t} = \frac{\mathbf{s}_\infty(t+\Delta t) - \mathbf{s}_\infty(t)}{\Delta t},$$

equations (8) and (9) provide the recursive relations

$$q_i^K(t+\Delta t) = q_i^K(t)\exp(-\Delta t/\tau_i) + \gamma_i^K \tau_i^K \frac{1-exp(-\Delta t/\tau_i)}{\Delta t}\Delta\sigma_\infty^o \tag{10}$$

$$\boldsymbol{q}_i^\mu(t+\Delta t) = \boldsymbol{q}_i^\mu(t)\exp(-\Delta t/\tau_i) + \gamma_i^\mu \tau_i^\mu \frac{1-exp\left(-\Delta t/\tau_i^\mu\right)}{\Delta t}\Delta\mathbf{s}_\infty \tag{11}$$

Then, through equations (4) and (5), the stresses at time $t+\Delta t$are given by

$$\sigma^o(t+\Delta t) = \sigma_\infty^o(t+\Delta t) + \sum_{i=1}^{N}\gamma_i^K\, exp\left(-\frac{t+\Delta t}{\tau_i^K}\right)\sigma_\infty^o(0) + \sum_{i=1}^{N} q_i^K\,(t+\Delta t) \tag{12}$$

$$\mathbf{s}(t+\Delta t) = \mathbf{s}_\infty(t+\Delta t) + \sum_{i=1}^{N}\gamma_i^\mu\, exp\left(-\frac{t+\Delta t}{\tau_i^\mu}\right)\mathbf{s}_\infty(0) + \sum_{i=1}^{N} \boldsymbol{q}_i^\mu\,(t+\Delta t) \tag{13}$$

which, using (10) and (11), can be written in the compact forms

$$\sigma^o(t+\Delta t) = H^K(t) + M^K\sigma_\infty^o(t+\Delta t) \tag{14}$$

$$\mathbf{s}(t+\Delta t) = \mathbf{H}^\mu(t) + M^\mu\mathbf{s}_\infty(t+\Delta t) \tag{15}$$

where

$$H^K(t) = \sum_{i=1}^{N} q_i^K(t)\exp\left(-\frac{\Delta t}{\tau_i^K}\right) + N^K\sigma_\infty^o(0) + (1-M^K)\sigma_\infty^o(t) \tag{16}$$

$$\mathbf{H}^\mu(t) = \sum_{i=1}^{N}\left[\mathbf{q}_i^\mu(t)\exp\left(-\frac{\Delta t}{\tau_i^\mu}\right)\right] + N^\mu\mathbf{s}_\infty(0) + (1-M^\mu)\mathbf{s}_\infty(t) \tag{17}$$

$$M^K = 1 + \sum_{i=1}^{N}\gamma_i^K\tau_i^K\frac{1-exp\left(-\frac{\Delta t}{\tau_i^K}\right)}{\Delta t}, M^\mu = 1 + \sum_{i=1}^{N}\gamma_i^\mu\tau_i^\mu\frac{1-exp\left(-\frac{\Delta t}{\tau_i^\mu}\right)}{\Delta t} \tag{18}$$

$$N^K = \sum_{i=1}^{N}\gamma_i^K exp\left(-\frac{t+\Delta t}{\tau_i^K}\right), \quad N^\mu = \sum_{i=1}^{N}\gamma_i^\mu exp\left(-\frac{t+\Delta t}{\tau_i^\mu}\right) \tag{19}$$

The total stress tensors at time $t+\Delta t$ is given by

$$\boldsymbol{\sigma}(t+\Delta t) = \sigma^o(t+\Delta t).\mathbf{1} + \mathbf{s}(t+\Delta t) \tag{20}$$

being $\mathbf{1}$ the second order unit tensor. By substituting the equations (14) and (15) into Eq. (20), the following relation is obtained:

$$\boldsymbol{\sigma}(t+\Delta t) = \mathbf{H}(t) + \mathbb{M} : \boldsymbol{\sigma}_\infty(t+\Delta t) \tag{21}$$

where

$$\mathbf{H}(t) = \sum_{i=1}^{N}\left[q_i^K(t)\exp\left(-\frac{\Delta t}{\tau_i^K}\right)\mathbf{1} + \mathbf{q}_i^\mu(t)\exp\left(-\frac{\Delta t}{\tau_i^\mu}\right)\right] + \mathbb{P} : \boldsymbol{\sigma}_\infty(t) + \mathbb{R} : \boldsymbol{\sigma}_\infty(0) \tag{22}$$

In (21) and (22), $\mathbb{M}$, $\mathbb{P}$ and $\mathbb{R}$ are fourth-order tensors defined by

$$\mathbb{M} = M^K \mathbb{J}_1 + M^\mu \mathbb{J}_2, \mathbb{P} = (1 - M^K)\mathbb{J}_1 + (1 - M^\mu)\mathbb{J}_2, \ \mathbb{R} = N^K \mathbb{J}_1 + N^\mu \mathbb{J}_2 \tag{23}$$

with

$$\mathbb{J}_1 = \frac{1}{3}\mathbf{1}\otimes\mathbf{1}, \quad \mathbb{J}_2 = \mathbb{I} - \frac{1}{3}\mathbf{1}\otimes\mathbf{1} \tag{24}$$

being $\mathbb{I}$ the fourth-order identity tensor. Equation (21) also can be written in the form

$$\boldsymbol{\sigma}(t + \Delta t) = \mathbf{H}(t) + \mathbb{C}^\infty : \boldsymbol{\varepsilon}(t + \Delta t) \tag{25}$$

where $\mathbb{C}^\infty = 3K_\infty M^K \mathbb{J}_1 + 2\mu_\infty M^\mu \mathbb{J}_2$.

3 NUMERICAL FORMULATION FOR THE VISCOELASTIC HOMOGENIZATION

Using the parametric FVDAM theory, the unit cell domain is discretized into quadrilateral subvolumes whose locations inside the unit cell are specified by their vertices referred to a fixed coordinate system (Cavalcante et al., 2007). Here, it is assumed that the periodic multiphase composite material is continuously reinforced along the y_1 axis so that the homogenization procedures require only the unit cell discretization in the y_2-y_3 plane. As shown in subsection 3.5, interface elements are used when the interphases are replaced by imperfect interfaces.

3.1 Subvolume Mapping and Displacement Field Representation

By the parametric FVDAM, the solution to the unit cell problem is generated by mapping a reference subvolume in the $\eta - \xi$ plane bounded by $-1 \leq \eta \leq 1$ and $-1 \leq \xi \leq 1$ onto a quadrilateral subvolume resident in the actual microstructure (Fig. 3) using the following coordinate transformations:

$$y_i(\eta, \xi) = \sum_{p=1}^{4} N_p(\eta, \xi) y_i^{(p)}, \quad (i = 2,3) \tag{26}$$

where $y_i^{(p)}$ denote the vertex coordinates of the subvolume and $N_p(\eta, \xi)$ are the interpolation function given by (Cavalcante et al., 2007)

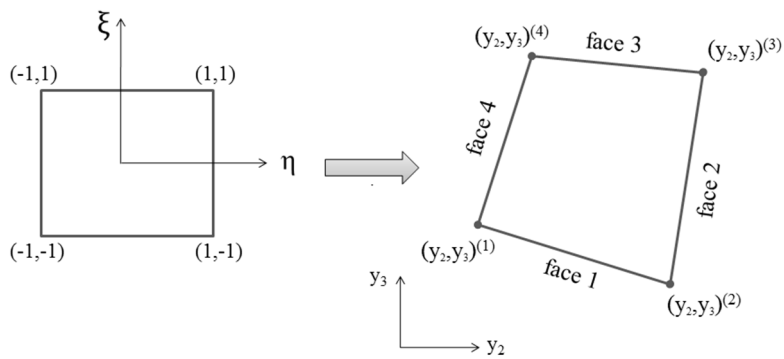

Figure 3: Mapping of the reference square subvolume onto a quadrilateral subvolume of the actual microstructure (after Cavalcante et al., 2007).

$$N_1(\eta,\xi)=\frac{1}{4}(1-\eta)(1-\xi), \qquad N_2(\eta,\xi)=\frac{1}{4}(1+\eta)(1-\xi)$$
$$N_3(\eta,\xi)=\frac{1}{4}(1+\eta)(1+\xi), \qquad N_4(\eta,\xi)=\frac{1}{4}(1-\eta)(1+\xi) \tag{27}$$

For homogenization of a composite material with periodic microstructure, the displacement field at time t in a subvolume can be represented by the two-scale expansion involving macroscopic and fluctuating components (Gattu et al., 2008)

$$u_i(t)=\bar{\varepsilon}_{ij}x_j+u_i'(t) \tag{28}$$

where $\bar{\varepsilon}_{ij}$ denote the macroscopic strain components, x_j are the point global coordinates and u_i' stand for the microstructure-induced fluctuating displacement components. Notice that in a relaxation test the macroscopic strains $\bar{\varepsilon}_{ij}$ are constant with respect to time. Using the standard version of the parametric FVDAM, the fluctuating components for each subvolume are approximated by polynomial expansions in the form

$$u_i'(t)=U_{i(00)}^t+\eta U_{i(10)}^t+\xi U_{i(01)}^t+\frac{1}{2}(3\eta^2-1)U_{i(20)}^t+\frac{1}{2}(3\xi^2-1)U_{i(02)}^t \tag{29}$$

being $i=1,2,3$ and $U_{i(mn)}^t$ denoting the unknown coefficients.

3.2 Surface-Averaged Strain-Displacement Relations

Considering the displacement field given in (29), the infinitesimal strain components for a subvolume are calculated by

$$\varepsilon_{ij}(t)=\bar{\varepsilon}_{ij}+\frac{1}{2}\left[\frac{\partial u_i'(t)}{\partial y_j}+\frac{\partial u_j'(t)}{\partial y_i}\right] \tag{30}$$

Introducing (29) into (30) and making the transformation of the Cartesian coordinates $(y_2,y_3)$to the parametric coordinates (η,ξ), the in-plane surface-averaged strain vectors at time t for the subvolume faces (Fig. 3) can be found by (for more details, see Cavalcante et al., 2007; Gattu et al. 2008)

$$\begin{bmatrix}\hat{\varepsilon}_{22}(t)\\ \hat{\varepsilon}_{33}(t)\\ 2\hat{\varepsilon}_{23}(t)\end{bmatrix}^{(2,4)}=\begin{bmatrix}\bar{\varepsilon}_{22}\\ \bar{\varepsilon}_{33}\\ 2\bar{\varepsilon}_{23}\end{bmatrix}+\bar{\mathbf{E}}\begin{bmatrix}\hat{\mathbf{J}} & \mathbf{0}\\ \mathbf{0} & \hat{\mathbf{J}}\end{bmatrix}\begin{bmatrix}\mathbf{A}_{1,2} & \mathbf{0}\\ \mathbf{0} & \mathbf{A}_{1,2}\end{bmatrix}\mathbf{U}_{\mathrm{in}}(\mathrm{t})$$
$$\begin{bmatrix}\hat{\varepsilon}_{22}(t)\\ \hat{\varepsilon}_{33}(t)\\ 2\hat{\varepsilon}_{23}(t)\end{bmatrix}^{(1,3)}=\begin{bmatrix}\bar{\varepsilon}_{22}\\ \bar{\varepsilon}_{33}\\ 2\bar{\varepsilon}_{23}\end{bmatrix}+\bar{\mathbf{E}}\begin{bmatrix}\hat{\mathbf{J}} & \mathbf{0}\\ \mathbf{0} & \hat{\mathbf{J}}\end{bmatrix}\begin{bmatrix}\mathbf{A}_{3,4} & \mathbf{0}\\ \mathbf{0} & \mathbf{A}_{3,4}\end{bmatrix}\mathbf{U}_{\mathrm{in}}(\mathrm{t}) \tag{31}$$

where $\mathbf{U}_{\mathrm{in}}(\mathrm{t})=\left[\mathrm{U}_{2(10)}^{\mathrm{t}}\mathrm{U}_{2(01)}^{\mathrm{t}}\mathrm{U}_{2(20)}^{\mathrm{t}}\ \mathrm{U}_{2(02)}^{\mathrm{t}}\mathrm{U}_{3(10)}^{\mathrm{t}}\mathrm{U}_{3(01)}^{\mathrm{t}}\mathrm{U}_{3(20)}^{\mathrm{t}}\ \mathrm{U}_{3(02)}^{\mathrm{t}}\right]^{\mathrm{T}}$, $\hat{\mathbf{J}}$ is the inverse of the volume-averaged Jacobian and

$$\bar{\mathbf{E}}=\begin{bmatrix}1 & 0 & 0 & 0\\ 0 & 0 & 0 & 1\\ 0 & 1 & 1 & 0\end{bmatrix},\quad \mathbf{A}_{1,2}=\begin{bmatrix}1 & 0 & \pm 3 & 0\\ 0 & 1 & 0 & 0\end{bmatrix},\quad \mathbf{A}_{3,4}=\begin{bmatrix}1 & 0 & 0 & 0\\ 0 & 1 & 0 & \pm 3\end{bmatrix} \tag{32}$$

Similarly, the out-of-plane surface-averaged strain vectors can be obtained by

$$\begin{bmatrix}2\hat{\varepsilon}_{12}(t)\\2\hat{\varepsilon}_{13}(t)\end{bmatrix}^{(2,4)} = \begin{bmatrix}2\bar{\varepsilon}_{12}\\2\bar{\varepsilon}_{13}\end{bmatrix} + \hat{\mathbf{J}}\mathbf{A}_{1,2}\mathbf{U}_{\text{out}}(\text{t})$$
$$\begin{bmatrix}2\hat{\varepsilon}_{12}(t)\\2\hat{\varepsilon}_{13}(t)\end{bmatrix}^{(1,3)} = \begin{bmatrix}2\bar{\varepsilon}_{12}\\2\bar{\varepsilon}_{13}\end{bmatrix} + \hat{\mathbf{J}}\mathbf{A}_{3,4}\mathbf{U}_{\text{out}}(\text{t}) \tag{33}$$

being $\mathbf{U}_{\text{out}}(\text{t}) = \left[\text{U}^{\text{t}}_{1(10)}\text{U}^{\text{t}}_{1(01)}\text{U}^{\text{t}}_{1(20)}\text{U}^{\text{t}}_{1(02)}\right]^{\text{T}}$.

3.3 Surface-Averaged Tractions

Using the Cauchy relations for a subvolume at time t, the tractions t_i are related to the stress components σ_{ji} by

$$t_i(t) = \sigma_{ji}(t)n_j \tag{34}$$

where n_j indicate the components of the outward unit normal vector to the subvolume faces (Fig. 3). Through equation (34) the in-plane surface-averaged tractions on each face f of a subvolume can be written in function of the corresponding in-plane surface-averaged stress components $\hat{\sigma}_{ji}$ by

$$\hat{\mathbf{t}}^{(f)}_{in} = \begin{bmatrix}\hat{t}_2\\\hat{t}_3\end{bmatrix}^{(f)} = \begin{bmatrix}n_2 & 0 & n_3\\0 & n_3 & n_2\end{bmatrix}^{(f)}\begin{bmatrix}\hat{\sigma}_{22}\\\hat{\sigma}_{33}\\\hat{\sigma}_{23}\end{bmatrix}^{(f)} \tag{35}$$

Similarly, the out-of-plane surface-averaged tractions are given by

$$\hat{\mathbf{t}}^{(f)}_{out} = [\hat{t}_1]^{(f)} = [n_2 \quad n_3]^{(f)}\begin{bmatrix}\hat{\sigma}_{12}\\\hat{\sigma}_{13}\end{bmatrix}^{(f)} \tag{36}$$

From equations (35) and (36), the in-plane and out-of-plane surface-averaged tractions on the four faces of a subvolume, $\hat{\mathbf{t}}_{in}$ and $\hat{\mathbf{t}}_{out}$, respectively, can be written in the general form

$$\hat{\mathbf{t}} = \begin{bmatrix}\hat{\mathbf{t}}^{(1)}\\\hat{\mathbf{t}}^{(2)}\\\hat{\mathbf{t}}^{(3)}\\\hat{\mathbf{t}}^{(4)}\end{bmatrix} = \mathbf{D}\begin{bmatrix}\widehat{\boldsymbol{\sigma}}^{(1)}\\\widehat{\boldsymbol{\sigma}}^{(2)}\\\widehat{\boldsymbol{\sigma}}^{(3)}\\\widehat{\boldsymbol{\sigma}}^{(4)}\end{bmatrix} \tag{37}$$

where

$$\widehat{\boldsymbol{\sigma}}^{(f)}_{in} = \begin{bmatrix}\hat{\sigma}_{22}\\\hat{\sigma}_{33}\\\hat{\sigma}_{23}\end{bmatrix}^{(f)}, \qquad \widehat{\boldsymbol{\sigma}}^{(f)}_{out} = \begin{bmatrix}\hat{\sigma}_{12}\\\hat{\sigma}_{13}\end{bmatrix}^{(f)} \tag{38}$$

and the matrices $\mathbf{D}_{in}$ and $\mathbf{D}_{out}$ are given in Appendix A.

From Eq. (25), the in-plane and out-of-plane surface-averaged stress components at time $t + \Delta t$ can be written, respectively, as follows:

$$\begin{bmatrix}\hat{\sigma}_{22}(t+\Delta t)\\\hat{\sigma}_{33}(t+\Delta t)\\\hat{\sigma}_{23}(t+\Delta t)\end{bmatrix}^{(f)} = \begin{bmatrix}\widehat{H}_{22}(t)\\\widehat{H}_{33}(t)\\\widehat{H}_{23}(t)\end{bmatrix}^{(f)} + \mathbf{C}^{\infty}_{\text{in}}\begin{bmatrix}\bar{\varepsilon}_{11}\\\hat{\varepsilon}_{22}(t+\Delta t)\\\hat{\varepsilon}_{33}(t+\Delta t)\\2\hat{\varepsilon}_{23}(t+\Delta t)\end{bmatrix}^{(f)} \tag{39}$$

$$\begin{bmatrix}\hat{\sigma}_{12}(t+\Delta t)\\ \hat{\sigma}_{13}(t+\Delta t)\end{bmatrix}^{(f)} = \begin{bmatrix}\hat{H}_{12}(t)\\ \hat{H}_{13}(t)\end{bmatrix}^{(f)} + \mathbf{C}^{\infty}_{\text{out}}\begin{bmatrix}2\hat{\varepsilon}_{12}(t+\Delta t)\\ 2\hat{\varepsilon}_{13}(t+\Delta t)\end{bmatrix}^{(f)}$$

being

$$\mathbf{C}^{\infty}_{\text{in}} = \begin{bmatrix} \mathrm{K}_{\infty}\mathrm{M}^{\mathrm{k}} - \frac{2}{3}\mu_{\infty}\mathrm{M}^{\mu} & \mathrm{K}_{\infty}\mathrm{M}^{\mathrm{k}} + \frac{4}{3}\mu_{\infty}\mathrm{M}^{\mu} & \mathrm{K}_{\infty}\mathrm{M}^{\mathrm{k}} - \frac{2}{3}\mu_{\infty}\mathrm{M}^{\mu} & 0 \\ \mathrm{K}_{\infty}\mathrm{M}^{\mathrm{k}} - \frac{2}{3}\mu_{\infty}\mathrm{M}^{\mu} & \mathrm{K}_{\infty}\mathrm{M}^{\mathrm{k}} - \frac{2}{3}\mu_{\infty}\mathrm{M}^{\mu} & \mathrm{K}_{\infty}\mathrm{M}^{\mathrm{k}} + \frac{4}{3}\mu_{\infty}\mathrm{M}^{\mu} & 0 \\ 0 & 0 & 0 & \mu_{\infty}\mathrm{M}^{\mu} \end{bmatrix}$$
$$\mathbf{C}^{\infty}_{\text{out}} = \begin{bmatrix}\mu_{\infty}\mathrm{M}^{\mu} & 0\\ 0 & \mu_{\infty}\mathrm{M}^{\mu}\end{bmatrix} \tag{40}$$

Introducing (39) into (37), for the time $t+\Delta\mathrm{t}$, the following relations between the surface-averaged tractions and strain components of a subvolume can be obtained:

$$\hat{\mathbf{t}}(t+\Delta t) = \mathbf{D}\hat{\mathbf{H}}(t) + \mathbf{D}\mathbf{C}\hat{\boldsymbol{\varepsilon}}(t+\Delta t) \tag{41}$$

where the matrices $\hat{\mathbf{H}}_{in}$, $\hat{\mathbf{H}}_{out}$, $\mathbf{C}_{in}$ and $\mathbf{C}_{out}$ are presented in Appendix A and

$$\hat{\boldsymbol{\varepsilon}} = [\hat{\boldsymbol{\varepsilon}}^{(1)} \quad \hat{\boldsymbol{\varepsilon}}^{(2)} \quad \hat{\boldsymbol{\varepsilon}}^{(3)} \quad \hat{\boldsymbol{\varepsilon}}^{(4)}]^{T} \tag{42}$$

with

$$\hat{\boldsymbol{\varepsilon}}^{(f)}_{in} = \begin{bmatrix}\bar{\varepsilon}_{11}\\ \hat{\varepsilon}_{22}\\ \hat{\varepsilon}_{33}\\ 2\hat{\varepsilon}_{23}\end{bmatrix}^{(f)}, \quad \hat{\boldsymbol{\varepsilon}}^{(f)}_{out} = \begin{bmatrix}2\hat{\varepsilon}_{12}\\ 2\hat{\varepsilon}_{13}\end{bmatrix}^{(f)} \tag{43}$$

Introducing (31) and (33) into (41), the following relations between the surface-averaged tractions and unknown coefficients of the fluctuating displacement fields are obtained

$$\hat{\mathbf{t}}(t+\Delta t) = \mathbf{D}\hat{\mathbf{H}}(t) + \mathbf{N}\mathbf{C}^{\infty}\bar{\boldsymbol{\varepsilon}} + \bar{\mathbf{A}}\mathbf{U}(t+\Delta t) \tag{44}$$

where $\bar{\boldsymbol{\varepsilon}}_{in} = [\bar{\varepsilon}_{11} \quad \bar{\varepsilon}_{22} \quad \bar{\varepsilon}_{33} \quad 2\bar{\varepsilon}_{23}]^{\mathrm{T}}$ and $\bar{\boldsymbol{\varepsilon}}_{out} = [2\bar{\varepsilon}_{12} \quad 2\bar{\varepsilon}_{13}]^{\mathrm{T}}$ and the matrices $\mathbf{N}_{in}$, $\mathbf{N}_{out}$, $\bar{\mathbf{A}}_{in}$ and $\bar{\mathbf{A}}_{out}$ can be seen in Appendix A. The matrices $\mathbf{C}^{\infty}$ for in-plane and out-of-plane cases are given in (40).

3.4 Equilibrium Equations and Subvolume Stiffness Matrix

The surface integral version of the equilibrium equations of a subvolume involving the surface-averaged tractions at time t+Δt are given by

$$\sum_{f=1}^{4}\hat{\mathbf{t}}(t+\Delta t)^{(f)}\,L_f = \mathbf{0} \tag{45}$$

where $\hat{\mathbf{t}}^{(f)}$ and L_f indicate the vector of surface-averaged tractions and the length of the subvolume face f, respectively. Introducing (44) into (45) and using (29), the following general expression can be found for the zeroth order coefficients of the fluctuating displacement fields:

$$\mathbf{U}_{00}(t+\Delta t) = \mathbf{\Phi}^{-1}\left[\mathbf{L}\mathbf{D}\hat{\mathbf{H}}(t) + \boldsymbol{\omega}\bar{\boldsymbol{\varepsilon}} + \boldsymbol{\theta}\hat{\mathbf{u}}'(t+\Delta t)\right] \tag{46}$$

where $\hat{\mathbf{u}}' = \left[\hat{\boldsymbol{u}}'^{(1)}\hat{\boldsymbol{u}}'^{(2)}\hat{\boldsymbol{u}}'^{(3)}\hat{\boldsymbol{u}}'^{(4)}\right]^{\mathrm{T}}$ and, for in-plane loading, $\mathbf{U}_{00}(\mathrm{t}+\Delta\mathrm{t}) = \left[\mathrm{U}_{2(00)}^{\mathrm{t}+\Delta\mathrm{t}} \quad \mathrm{U}_{3(00)}^{\mathrm{t}+\Delta\mathrm{t}}\right]^{\mathrm{T}}$ and $\hat{\mathbf{u}}'^{(f)} = \left[\hat{u}_2'^{(f)}\hat{u}_3'^{(f)}\right]^{\mathrm{T}}$, while for out-of-plane loading, $\mathbf{U}_{00}(\mathrm{t}+\Delta\mathrm{t}) = \left[\mathrm{U}_{1(00)}^{\mathrm{t}+\Delta\mathrm{t}}\right]$ and $\hat{\mathbf{u}}'^{(f)} = \left[\hat{u}_1'^{(f)}\right]$. The matrices $\mathbf{\Phi}$, $\boldsymbol{\omega}$, $\boldsymbol{\theta}$ and $\mathbf{L}$ are presented in Appendix A.

Using (46) and (29), the vector $\mathbf{U}(\mathrm{t}+\Delta\mathrm{t})$ is determined in function of the vector of surface-averaged fluctuating displacements $\hat{\mathbf{u}}'$ and, then, Eq. (44) can be rewritten in the form

$$\hat{\mathbf{t}}(t+\Delta t) = \mathbf{S}\bar{\boldsymbol{\varepsilon}} + \mathbf{F}\hat{\mathbf{H}}(t) + \mathbf{K}\hat{\mathbf{u}}'(t+\Delta t) \tag{47}$$

where $\mathbf{K} = \overline{\mathbf{A}}\overline{\mathbf{B}}$ is the subvolume stiffness matrix. The matrices $\overline{\mathbf{B}}$, $\mathbf{S}$ and $\mathbf{F}$ for in-plane and out-of-plane loadings are given in the Appendix A.

3.5 Viscoelastic Imperfect Interface Element

Figure 4 shows an arbitrarily curved linear viscoelastic isotropic thin interphase of constant thickness h located between a fiber and the matrix of a composite material. The displacements and tractions are assumed as continuous across the matrix/interphase and fiber/interphase interfaces, what is referred to as perfect interfaces. On the contrary, when these continuity conditions of tractions or displacements do not exist across an interface, it is named as imperfect interface. It can be found in the literature studies on the possible substitution of a thin interphase for an equivalent imperfect interface with appropriate discontinuities in tractions and displacements (Benveniste,2006, Hashin, 2002). This strategy allows to analyze a three-phase material (matrix, fiber and interphase) using an equivalent two-phase material (matrix, fiber and interface), as shown in Fig. 4.

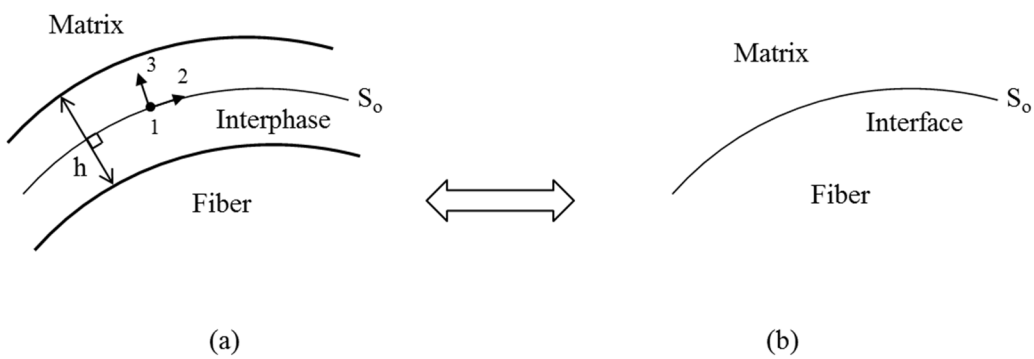

Figure 4: (a) Interphase between fiber and matrix and b) equivalent imperfect interface.

Here, a viscoelastic imperfect interface element is derived based on the idea of replacing the thin interphase by an imperfect interface, positioned at the location of the middle surface S_o (see Fig. 4), across the which are imposed continuity in tractions and appropriate displacement jumps related to their associated traction components. These interface conditions are demonstrated to be adequate when the interphase has stiffness much smaller than the other two composite phases (matrix and fiber).

For the case of linear viscoelastic interphase, the traction components can be written as follows (Hashin, 1991):

$$t_i(t) = D_i(t)[u_i(0)] + \int_0^t D_i(t-s)\frac{\partial}{\partial s}[u_i(s)]ds \qquad (i = 1,2,3) \tag{48}$$

being $\mathrm{D_i}$ the viscoelastic interface functions and the directions 1, 2 and 3 are shown in Fig. 4, where 1 and 2 are the tangential directions and 3 is the normal direction. The symbol [ ] is used to represent displacement jumps across the interface, so that

$$[u_i(t)] = u_i^+(t) - u_i^-(t) \tag{49}$$

where the signals + and − indicate the interface sides adjacent to the matrix and fiber, respectively.

For a linear viscoelastic interphase obeying a generalized Maxwell model, the interface functions are given by

$$D_{\mathrm{i}}(t) = D_{i\infty} + \sum_{j=1}^{N} D_{ij}\exp(-\mathrm{t}/\tau_{ij}) \tag{50}$$

being $D_{\mathrm{i}\infty}$ and D_{ij} the elastic constants corresponding to the springs and τ_{ij} are the relaxation times related to the direction i and j-th Maxwell branch of the model. Introducing (50) into (48), the following expression can be found:

$$t_i(t) = \sum_{j=1}^{N} q_{ij}(t) + D_{i\infty}\sum_{j=1}^{N}\gamma_{ij}\exp\left(-\frac{\mathrm{t}}{\tau_{ij}}\right)[u_i(0)] + D_{i\infty}[u_i(t)] \tag{51}$$

where $\gamma_{ij} = D_{ij}/D_{i\infty}$ and q_{ij} are internal variables defined by

$$q_{ij}(t) = \int_0^t D_{ij}exp\left(-\frac{t-s}{\tau_{ij}}\right)\left[\frac{\partial u_i(s)}{ds}\right]ds \tag{52}$$

Considering small time step Δt and using an incremental procedure similar to that used to derive (10), one can obtain from Eq. (52) the recursive expression for the internal variables

$$q_{ij}(t+\Delta t) = \exp\left(-\frac{\Delta t}{\tau_{ij}}\right)q_{ij}(t) + \frac{\eta_{ij}}{\Delta t}\left[1-\exp\left(-\frac{\Delta t}{\tau_{ij}}\right)\right]([u_i(t+\Delta t)] - [u_i(t)]) \tag{53}$$

being $\eta_{ij} = D_{ij}\tau_{ij}$ (no summation) the dashpot constant corresponding to the direction i and the j-th Maxwell element of the viscoelastic model. Using the equations (51) and (53), the traction components at time $t + \Delta t$ can be written in the form

$$t_i(t+\Delta t) = M_i(t) + Q_i(t)[u_i(0)] + R_i[u_i(t)] + K_i[u_i(t+\Delta t)] \tag{54}$$

with

$$M_i(t) = \sum_{j=1}^{N}\exp\left(-\frac{\Delta \mathrm{t}}{\tau_{ij}}\right)q_{ij}(t), \qquad Q_i(t) = D_{i\infty}\sum_{j=1}^{N}\gamma_{ij}\exp\left(-\frac{t+\Delta t}{\tau_{ij}}\right) \tag{55}$$

$$R_i = -\sum_{j=1}^{N} \frac{\eta_{ij}}{\Delta t}\left[1 - \exp\left(-\frac{\Delta t}{\tau_{ij}}\right)\right], \qquad K_i = D_{i\infty} - R_i$$

As the parametric finite-volume formulation employs quadrilateral subvolumes for discretization of fiber and matrix, the interfaces are discretized into straight line segments as shown in Fig. 5. Using Eq. (54), the surface-averaged traction vector of the interface element at time $t + \Delta t$ can be expressed as

$$\hat{\mathbf{t}}_{\mathrm{I}}(t + \Delta t) = \mathbf{H}_{\mathrm{I}}(t) + \mathbf{K}_{\mathrm{I}}\hat{\mathbf{u}}_{\mathrm{I}}(t + \Delta t) \tag{56}$$

where $\hat{\mathbf{t}}_{\mathrm{I}} = [\hat{t}_1\hat{t}_2\hat{t}_3]^{\mathrm{T}}$, $\hat{\mathbf{u}}_{\mathrm{I}} = [\hat{u}_1^-\hat{u}_2^-\hat{u}_3^-\hat{u}_1^+\hat{u}_2^+\hat{u}_3^+]^{\mathrm{T}}$, $\mathbf{K}_{\mathrm{I}}$ is the interface element stiffness matrix and $\mathbf{H}_{\mathrm{I}}(\mathrm{t}) = \mathbf{Q}(\mathrm{t})\hat{\mathbf{u}}_{\mathrm{I}}(0) + \mathbf{M}(\mathrm{t}) + \mathbf{R}\hat{\mathbf{u}}_{\mathrm{I}}(\mathrm{t})$. The matrices $\mathbf{L}$, $\mathbf{M}$, $\mathbf{R}$ and $\mathbf{K}_{\mathrm{I}}$ are shown in the Appendix B. Notice that $\hat{t}_i^- = \hat{t}_i^+$.

Here, $\hat{u}_i^-$ and $\hat{u}_i^+$ indicate the surface-averaged displacement components on the two interface sides $-$ and $+$, respectively. It is worth noting that, in accordance with Eq. (28), $[u_i(\mathrm{t})] = [u_i'(t)] = u_i'^+(t) - u_i'^-(t)$ for any time t. Then, the vector $\hat{\mathbf{u}}_{\mathrm{I}}$ appearing in Eq. (56) can be substituted by the corresponding surface-averaged fluctuation displacement vector $\hat{\mathbf{u}}_{\mathrm{I}}'$.

For the case of isotropic interphase with linear viscoelastic effect restricted to shear, the viscoelastic interface functions can be expressed as

$$\mathrm{D}_1(t) = \mathrm{D}_2(t) = \frac{G_I(t)}{h}, \qquad \mathrm{D}_3(t) = \frac{1}{h}\left[K_{\mathrm{I}} + \frac{4}{3}G_{\mathrm{I}}(t)\right] \tag{57}$$

where K_{I} and $G_{\mathrm{I}}(\mathrm{t})$ are the elastic Bulk modulus and the relaxation shear function of the interphase material, respectively.

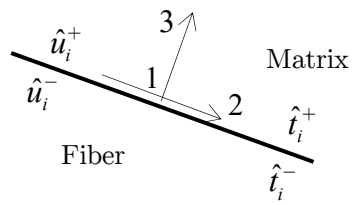

Figure 5: Interface element.

3.6 Assembly of the Global System of Equations

The surface-averaged tractions on the local faces of each subvolume and interface elements of the unit cell are related to the corresponding surface-averaged fluctuating displacements through the local stiffness matrices, as shown in (47) and (56), respectively. The local stiffness matrices are assembled into global systems of equations by applying surface-averaged interfacial fluctuating displacements and tractions compatibility conditions, followed by the specified boundary conditions.

This approach is based on an appropriate global face numbering system, in which each internal local face has a corresponding global face number, common to the adjacent subvolumes or subvolume and interface element, while the external faces of subvolumes along the opposite unit cell

boundaries are numbered taking into account the periodicity conditions. These external faces, with similar fluctuating displacement distributions imposed by the periodicity conditions, receive common face numbers.

The procedure for assembling the global systems is similar to that used in the finite-element algorithms. In these later, the degrees of freedom are associated with the element nodes, while in the present finite-volume formulation they are referred to the subvolume and interface element faces.

Imposing compatibility conditions of tractions and surface-averaged fluctuating displacements on the common interfaces, as well as, the specified boundary conditions, the global systems of equations takes the following forms for the in-plane and out-of-plane, respectively:

$$\mathbf{K}_{in}^{G}\widehat{\mathbf{U}}_{in}'(t+\Delta t)=\Delta\mathbf{C}_{in}\bar{\boldsymbol{\varepsilon}}_{in}+\mathbf{G}_{in}(t)\mathbf{K}_{out}^{G}\widehat{\mathbf{U}}_{out}'(t+\Delta t)=\Delta\mathbf{C}_{out}\bar{\boldsymbol{\varepsilon}}_{out}+\mathbf{G}_{out}(t) \tag{58}$$

where $\widehat{\mathbf{U}}'$ represents the unknown global surface-averaged fluctuation displacement vectors and $\mathbf{K}^{G}$ stands for the global stiffness matrices. The global $\Delta\mathbf{C}$ matrices are comprised of the differences in the material stiffness matrices of adjacent subvolumes and $\mathbf{G}$ contains known surface-averaged viscoelastic strain contributions. To eliminate the singularity of the systems (58), the four corner subvolume faces of the unit cell are constrained. The solutions of these systems enable the calculation of the fluctuating displacement coefficients and thus displacement, strain and stress fields in each subvolume for the time step.

3.7 Homogenization Procedures

Composite materials with linear viscoelastic phases exhibit effective linear viscoelastic behaviors (Hashin, 1965, 1970a). Then, the effective constitutive relation for these materials can be written in the form

$$\sigma_{ij}^{*}(t)=C_{ijkl}^{*}(t)\varepsilon_{ij}^{*}(0)+\int_{0}^{t}C_{ijkl}^{*}(t-s)\frac{d\varepsilon_{ij}^{*}(s)}{ds}ds \tag{59}$$

where σ_{ij}^{*} and ε_{ij}^{*} are the effective unit cell stress and strain components, respectively, and C_{ijkl}^{*} indicate the material homogenized relaxation functions. For the particular case of relaxation test, with imposed macroscopic constant strain components $\bar{\varepsilon}_{kl}$, the effective stresses are given by

$$\sigma_{ij}^{*}(t)=C_{ijkl}^{*}(t)\bar{\varepsilon}_{kl} \tag{60}$$

The subvolume-averaged strains $\bar{\varepsilon}_{ij}^{(q)}$ of the q-th subvolume in the discretized unit cell are related to the macroscopic strains by the expression

$$\bar{\varepsilon}_{ij}^{(q)}(t)=A_{ijkl}^{(q)}(t)\bar{\varepsilon}_{kl} \tag{61}$$

being $A_{ijkl}^{(q)}$ the subvolume strain concentration tensor components. The subvolume-averaged strains and stresses of a subvolume q with volume Ω_q are defined by the relations

$$\bar{\varepsilon}_{ij}^{(q)}(t)=\frac{1}{\Omega_q}\int_{\Omega_q}\varepsilon_{ij}(t)d\Omega_q,\qquad \bar{\sigma}_{ij}^{(q)}(t)=\frac{1}{\Omega_q}\int_{\Omega_q}\sigma_{ij}(t)d\Omega_q \tag{62}$$

Using the definition of effective unit cell stress, the following expression can be readily derived:

$$\sigma_{ij}^{*}(t) = \sum_{q=1}^{N_q} v^{(q)} \bar{\sigma}_{ij}^{(q)}(t) \tag{63}$$

where N_q is the total number of subvolumes in the discretized unit cell and $v^{(q)}$ the volume fraction of the subvolume q, i.e., $v^{(q)} = \Omega_q/\Omega$, being Ω the unit cell volume.

Using the relations (25), (61) and (63), the effective stresses at time $t + \Delta t$ can be written in the form

$$\sigma_{ij}^{*}(t+\Delta t) = \sum_{q=1}^{N_q} v^{(q)} \left[\bar{H}_{ij}^{(q)}(t) + C_{ijkl}^{\infty(q)} A_{klmn}^{(q)}(t+\Delta t) \bar{\varepsilon}_{mn} \right] \tag{64}$$

where $\bar{H}_{ij}^{(q)}$ indicates the subvolume-averaged components of the tensor **H** defined in (22). Considering that $\bar{H}_{ij}^{(q)}(t) = 0$ at $t < 0$ and using (60) together with (64), the homogenized elastic stiffness tensor can be obtained as

$$C_{ijmn}^{*}(0) = \sum_{q=1}^{N_q} v^{(q)} C_{ijkl}^{\infty(q)} A_{klmn}^{(q)}(0) \tag{65}$$

Considering that the internal stress variables are null at time $t = 0$, it follows from Eq. (22) the relation

$$\bar{H}_{ij}^{(q)}(0) = \left(P_{ijkl}^{(q)} + R_{ijkl}^{(q)} \right) \bar{\sigma}_{\infty kl}^{(q)}(0) \tag{66}$$

where $P_{ijkl}^{(q)}$ and $R_{ijkl}^{(q)}$ are the components of the tensors $\mathbb{P}$ and $\mathbb{R}$, respectively, for the q-th subvolume.

The homogenized relaxation functions at any time $t + \Delta t$ can be computed in an incremental way using the following recursive expression:

$$C_{ijkl}^{*}(t+\Delta t)\bar{\varepsilon}_{kl} = \sum_{q=1}^{N_q} v^{(q)} \left[\bar{H}_{ij}^{(q)}(t) + C_{ijkl}^{\infty(q)} A_{klmn}^{(q)}(t+\Delta t) \bar{\varepsilon}_{mn} \right] \tag{67}$$

once that all the terms appearing on the right side are previously known. The homogenized relaxation functions at time $t + \Delta t$ are calculated by solving the systems (58) for six independent elementary macroscopic strain states. In each case, only a single unit strain component $\bar{\varepsilon}_{ij}\,(i \geq j)$ is applied, while the other strain components are kept to zero. For instance, Case 1: $\bar{\varepsilon}_{11} = 1$ with all other components $\bar{\varepsilon}_{ij} = 0$; Case 2: $\bar{\varepsilon}_{12} = 1$ with all other components $\bar{\varepsilon}_{ij} = 0$; and so on. For each elementary strain loading, the solutions of (58) enable the evaluation of $\bar{\varepsilon}_{ij}^{(q)}(t+\Delta t)$ for all subvolumes resident in the unit cell domain and, consequently, the corresponding set of homogenized relaxation functions can be evaluated through (67).

Using the above described numerical procedure, the homogenized relaxation functions are evaluated at a set of discrete times t_n defined by the selected Δt values. In the examples shown in the next section, Prony series are used for interpolation of the discrete points.

3.8 Application to Large Displacement Problems

An important role of the micromechanics theories is the evaluation of the material effective properties for subsequent use as input data for the computation of the macroscopic behavior of structures and other systems constituted by the same composite material. In the case of macro mechanics behavior involving geometrical nonlinearities, the analysis usually employs specialized energetically conjugate measures of strain and stress. For instance, in Lagrangian material description framework, it is common the use of the second Piola-Kirchhoff stress tensor together with the Green-Lagrange strain tensor, or the first Piola-Kirchhoff stress tensor with the deformation gradient tensor(Bathe, 2014).

As mentioned above, the presented formulation has been particularly derived for homogenization of viscoelastic periodic materials in the range of small displacements. Despite this fact, the homogenized relaxation functions obtained by (67) may be employed in incremental viscoelastic macro mechanics analysis involving large displacements with small strains and based on the second Piola-Kirchhoff stress and Green-Lagrange strain tensors. This is justified by the invariance of these stress and strain measures with respect to the rigid body motion, what implies that any material description formulated for infinitesimal displacement range using engineering stress and strain tensors can readily be applied to large displacement with small strain analysis, provided the second Piola-Kirchhoff stress and Green-Lagrange strain tensors are used.

On the other hand, the unit cell boundary-value problem corresponding to the homogenization approach described herein can be more convenient derived using the first Piola-Kirchhoff stress and the deformation gradient tensor, what enables to apply homogenous boundary conditions and write the equilibrium equations in a more direct and physically clearer manner. This is also pointed out by Cavalcante & Pindera (2014a) in the case of a homogenization framework derived for hyperelastic periodic materials undergoing finite deformations using the generalized FVDAM. The derivation of the unit cell boundary-value problem for homogenization of viscoelastic periodic composite materials under large displacement domain is out of the scope of the present work.

4 NUMERICAL RESULTS

4.1 Composite Material with Viscoelastic Matrix and Elastic Fibers

The objective of this first example is to demonstrate the capability of the proposed model to describe the homogenized relaxation behavior of a two-phase composite material. The material has a periodic microstructure constituted by a linear viscoelastic isotropic matrix reinforced by unidirectional elastic long fibers with volume fraction $v_f = 0.54$.

The viscoelastic matrix behavior is characterized by a Maxwell model with Young's modulus $E_m = 3.27$ MPa, dashpot modulus $\eta_m = 300\ \mathrm{GPa} \cdot \mathrm{hr}$ and constant Poisson ratio $\nu_m = 0.38$. On the other hand, the fiber elastic properties are $E_f = 68.67$ MPa and $\nu_f = 0.21$.

To verify the performance of the homogenization model with respect to the convergence, three square meshes with different refinement degrees (coarse, medium and fine) were used for the unit cell discretization (Fig. 6). Six hundred incremental steps with a time interval $\Delta t = 10\ \mathrm{sec}$ were made for each analysis. The results obtained for the homogenized relaxation functions C^*_{1212} and C^*_{2222} are illustrated in Figures 7 and 8, respectively, compared with analytical solutions obtained

by Luciano and Barbero (1995) and Debotton and Tevet-Deree (2004). The former authors employed the Periodic Microstructure Method to derive closed-form expressions in the Laplace domain for the homogenized relaxation functions of periodic composite materials with square array of infinitely long elastic fibers in a linear viscoelastic matrix. The inversion to the time domain is carried out analytically for the case of viscoelastic matrix whose behavior can be represented by a Maxwell model connected in series to a Kelvin-Voigt model. On the other hand, Debotton and Tevet-Deree (2004) presented analytical equations in the time domain for the relaxation moduli of unidirectional fiber-reinforced composites with random array of linear elastic fibers embedded in a viscoelastic matrix whose behavior is elastic in dilatation and governed by a Zener model in shear.

As it can be seen in Figures 7 and 8, the rate of convergence of the effective moduli with the mesh refinement is very rapid and the calculated relaxation functions are in excellent agreement with the closed-form analytical results due to Luciano and Barbero (1995). The differences between the effective relaxation curves obtained using Debotton and Tevet-Deree (2004) and those corresponding to the other two solutions could be explained by the hypotheses related to the composite microstructures. The analytical expressions due to Debotton and Tevet-Deree (2004) were derived for composites with random array of fibers and, consequently, they are approximate for the cases of composites with periodic microstructures.

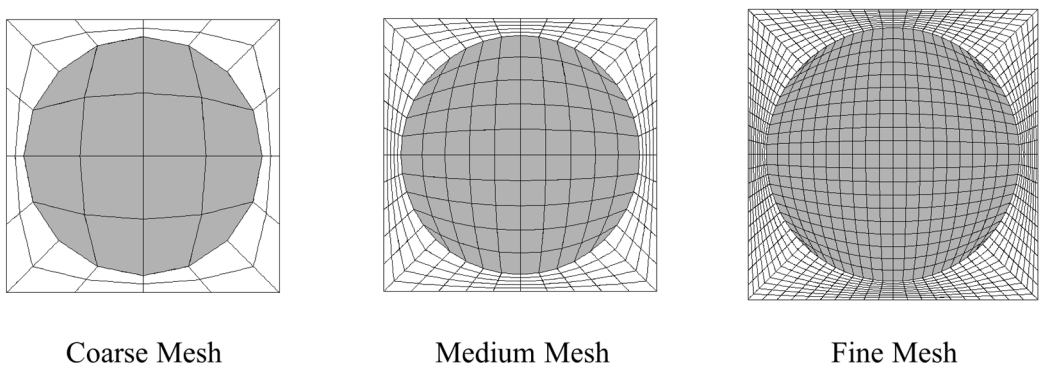

Figure 6: Unit cell discretizations for the fiber-reinforced composite material.

4.2 Composite Material with Viscoelastic Interphase

In this example, the proposed model is applied to investigate the influence of a thin viscoelastic interphase on the relaxation of the homogenized axial shear stiffness of a periodic fiber reinforced composite with linear elastic fibers and matrix. Fiber and matrix have the following elastic properties, respectively:

$$E_f = 193\ \text{GPa},\ \nu_f = 0.2$$
$$E_m = 62.7\ \text{GPa},\ \nu_m = 0.22$$

The fibers present a volume fraction of 50% and circular cross section with a radius $\mathrm{r} = 100\ \mu\text{m}$. The interphase has a thickness $\mathrm{h} = 20\ \text{nm}$ and its material is linear elastic in dilatation and linear viscoelastic in shear. This viscoelastic behavior is defined by a Maxwell model with the

following properties: $G_i = 1.608\times10^{-3}$ GPaand $\tau_i = 1$ hr. The Poisson's ratio is considered constant and given by $\nu_i = 0.375$.

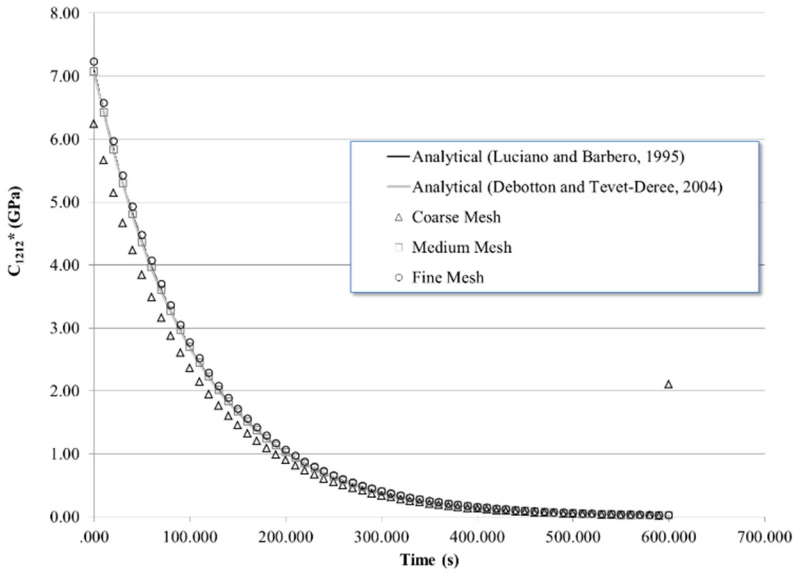

Figure 7: Homogenized relaxation function C^*_{1212} of the fiber-reinforced composite material.

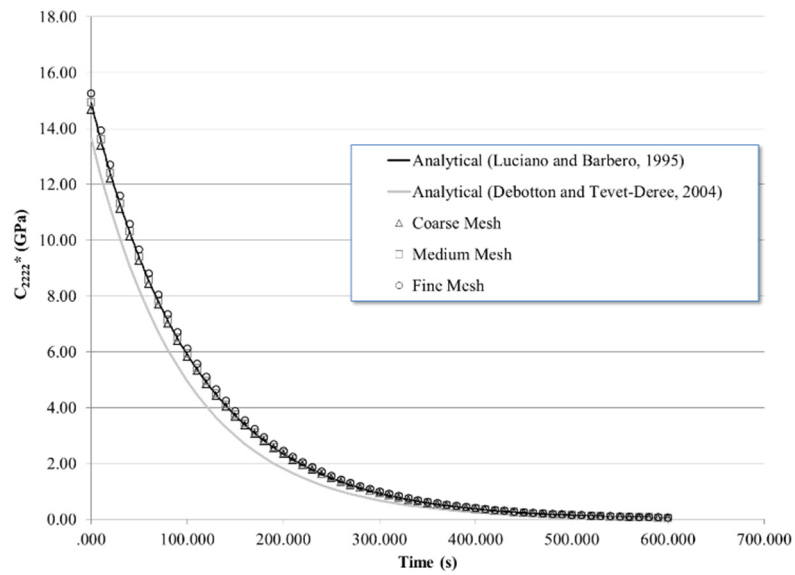

Figure 8: Homogenized relaxation function C^*_{2222} of the fiber-reinforced composite material.

The analyses included two different discretization cases: a) square unit cell with three constituent phases (matrix, interphase and fiber) and b) square unit cell with two phases (matrix and fiber) and imperfect interface. Figure 9 shows the results found for the homogenized axial shear relaxation curves $G^*_a(t)$ for the two discretization cases together with the analytical solution presented in Hashin (1991), which considers the case of a thin linear viscoelastic interphase between two elastic

components. This analytical solution is based on closed-form results for elastic composites with interphase and correspondence principle for linear viscoelastic materials. As it can be observed, the numerical results obtained by using the proposed viscoelastic imperfect interface model are in excellent agreement with those corresponding to three-phase unit cell, as well as, with the Hashin's analytical solution. The differences between the numerical and analytical solutions are also shown in Fig. 9. It is observed that the values of these differences, for the whole time interval, are smaller than 2%, what indicates the very good performance of the proposed viscoelastic model in relation to the closed-form analytical solution.

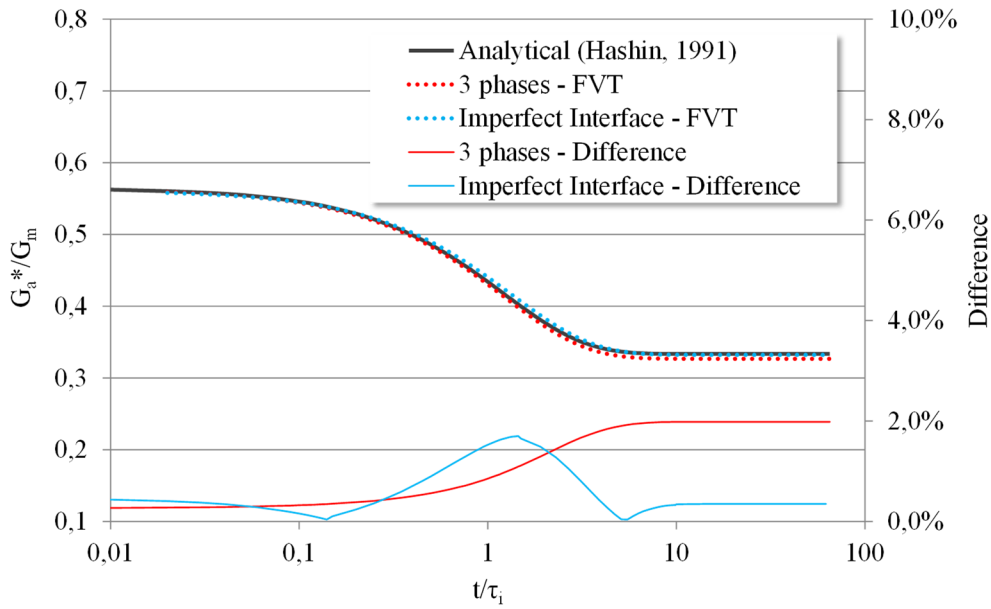

Figure 9: Effective axial shear relaxation function.

4.3 Viscoelastic Multilayers with Periodic Architecture and Interphases

In this example, the proposed homogenization model is applied to determine the effective relaxation functions of periodic multilayers comprised of alternating viscoelastic and elastic layers with elastic interphases between them. Multilayers with flat and sinusoidal wavy architectures are considered (Fig. 10(a)). The unit cell and its discretization employed in the analyses for the case of amplitude-to-wavelength ratio of 10% are shown in Fig. 10(b).

The material behavior of the viscoelastic layer is simulated by a generalized Maxwell model with the following properties: $E_\infty = 72.4$ GPa, $E_1 = 36.2$ GPa, $\eta_1 = 100\,\text{GPa}\cdot\text{sec}$ and Poisson's ratio constant $\nu = 0.3$. The reinforcing elastic layers present a volume fraction of 20% and elastic properties: $E = 420\,\text{GPa}$ and $\nu = 0.25$. The interphase has thickness $h = 20\,\text{nm}$ and elastic constants $G_i = kG_m$ and $\nu_i = 0.30$, where G_m is the shear elastic modulus of the viscoelastic layers and k is a variable parameter. Different values of k are assumed in order to investigate the range of the interphase stiffness for which the hypothesis of discontinuity in displacements and continuity in tractions across the interfaces provides consistent results when compared with the three phase unit

cell solutions. Figures 11 - 18 show the results of homogenized relaxation functions obtained by the proposed model for different values of k, considering two situations: a) three-phase unit cell (viscoelastic and elastic layers separated by the interphases) and b) two-phase unit cell (viscoelastic and elastic layers separated by imperfect interfaces).

Figures 11–14 show that, for the effective relaxation moduli C^*_{2222} and C^*_{1212}, the curves corresponding to the cases of three-phase unit cell and two-phase unit cell with imperfect interface are practically coincident for values of $k \leq k_{lim} \cong 10$ and, from this point, the mentioned curves exhibit a rapid and increasing separation.This means that the hypothesis of continuity in tractions and discontinuity in displacements, adopted for the derivation of the imperfect interface element, is not adequate for modeling of composites with interphases of high stiffness in relation to the other phases. The limit value of the interphase stiffness to applicability of the imperfect interface model depends on the composite features. In general, as commented in section 3.5, the hypothesis of continuity in tractions and discontinuity in displacements is adequate when the interphase material has stiffness small in relation to the other composite phases. The homogenized relaxation curves in Figures 15-18 also show the limitation of the imperfect interface model with respect to the values of k.

The influence of the wavy architecture on the stiffness of multilayers can also be observed by comparing the homogenized relaxation curves of the flat and wavy multilayers (Figures 15-18). As shown in these figures, the waviness can reduce substantiallythe stiffness of multilayers. This reduction is strongly dependent on the amplitude-to-wavelength ratio of the layers and interphase stiffness. It is shown from the results that the influence of the interphase stiffness is particularly very significant for the case of wavy multilayers.

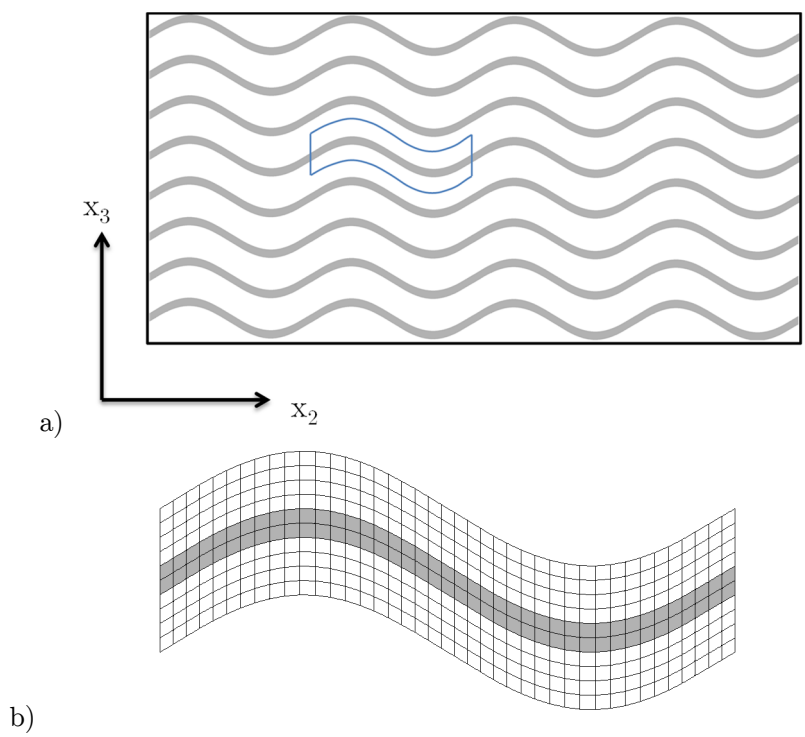

Figure 10: a) Periodic multilayer composite with sinusoidal wavy architecture and b) the repeating unit cell and its discretization.

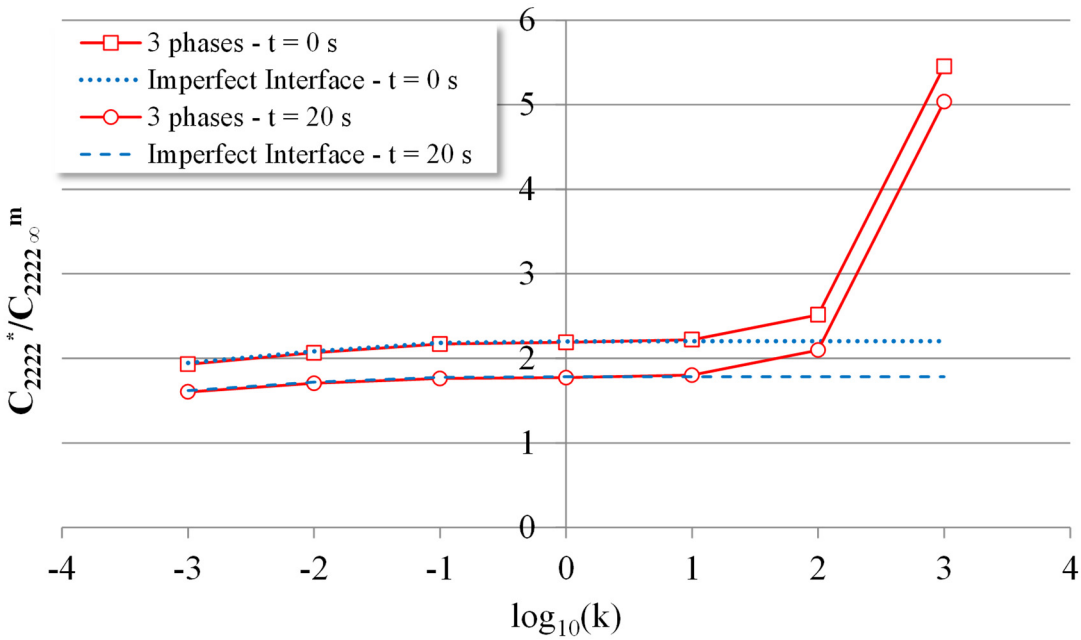

Figure 11: Variation of C_{2222}^{*} with the parameter $k = G_i/G_m$ for the flat multilayer.

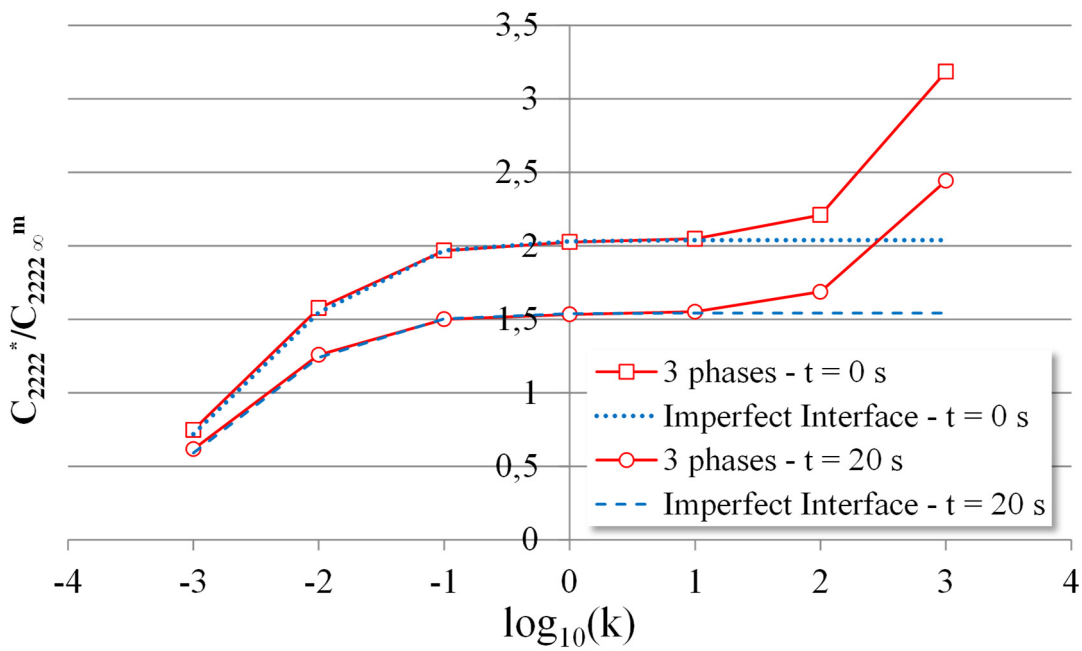

Figure 12: Variation of C_{2222}^{*} with the parameter $k = G_i/G_m$ for the wavy multilayer.

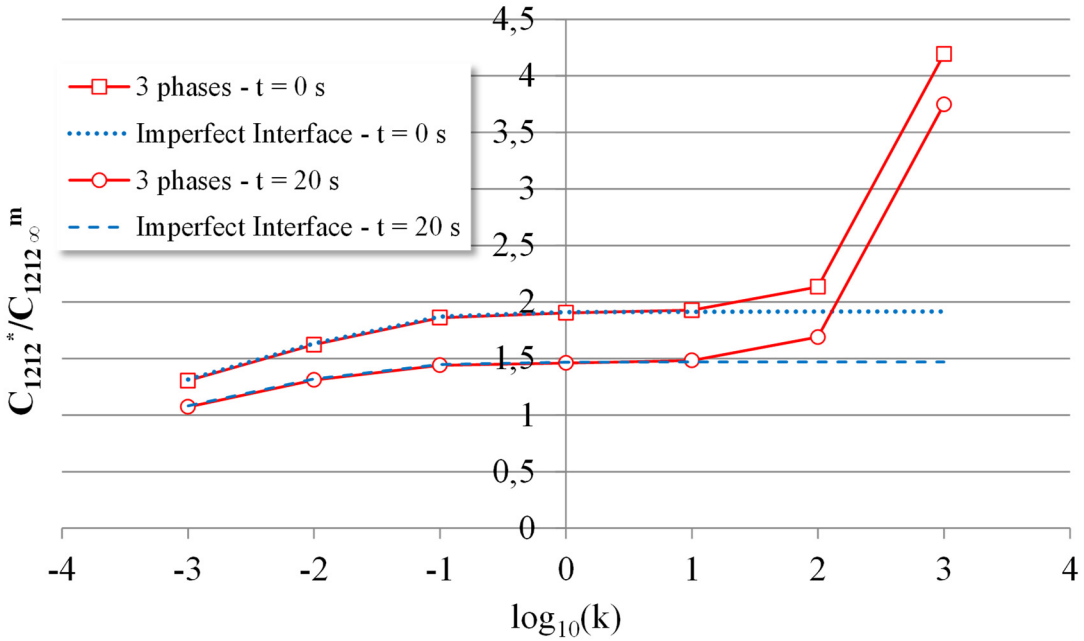

Figure 13: Variation of C_{1212}^{*} with the parameter $k = G_i/G_m$ for the flat multilayer.

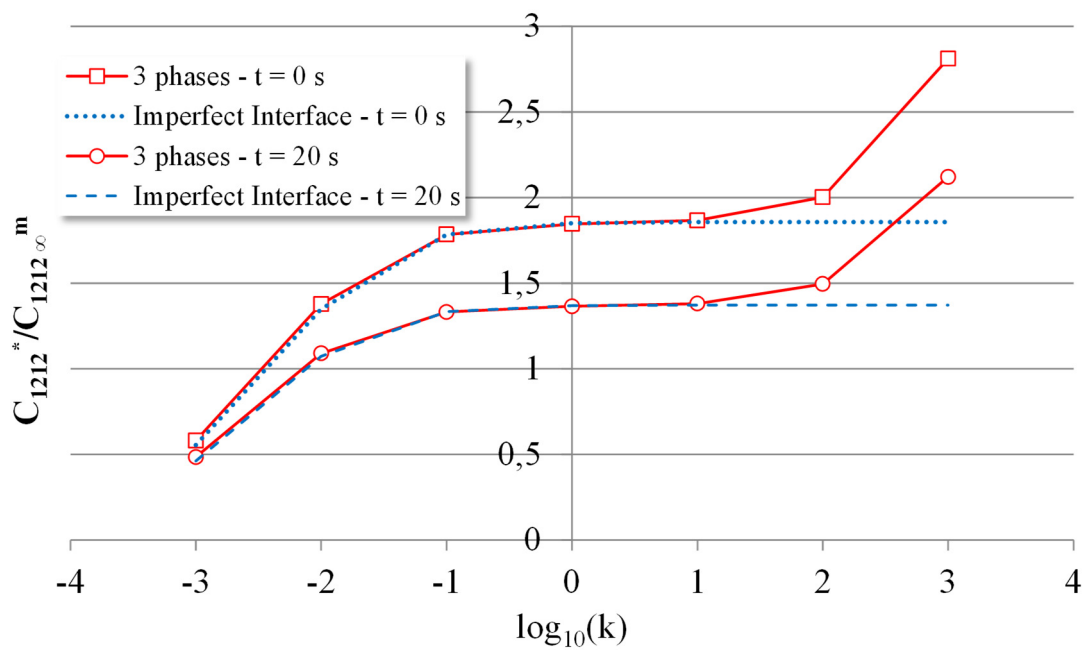

Figure 14: Variation of C_{1212}^{*} with the parameter $k = G_i/G_m$ for the wavy multilayer.

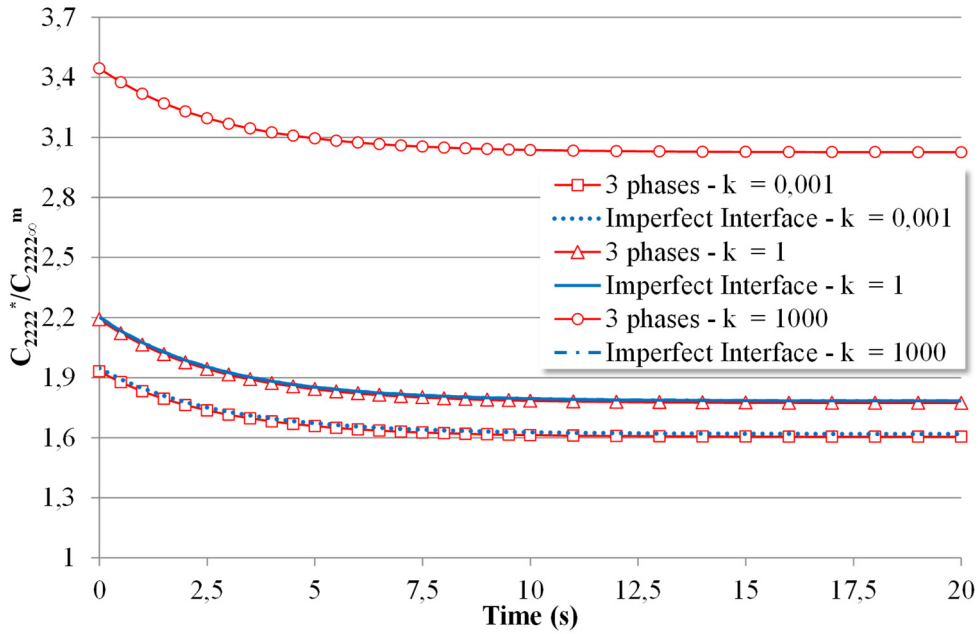

Figure 15: Homogenized relaxation function C_{2222}^{*} of the flat multilayer for different values of the ratio $k = G_i/G_m$.

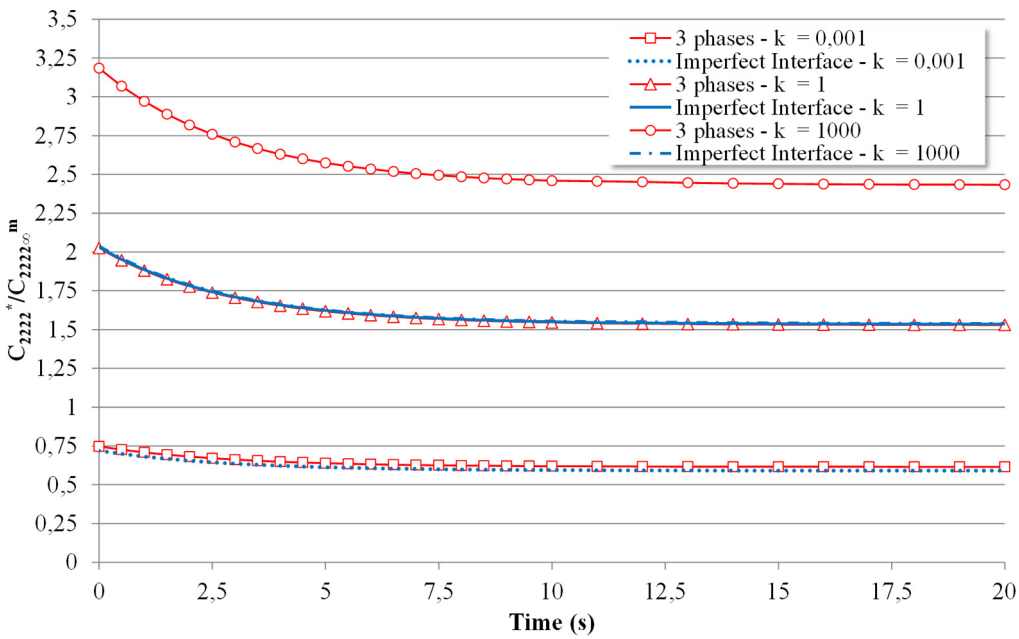

Figure 16: Homogenized relaxation function C_{2222}^{*} of the wavy multilayer for different values of the ratio $k = G_i/G_m$.

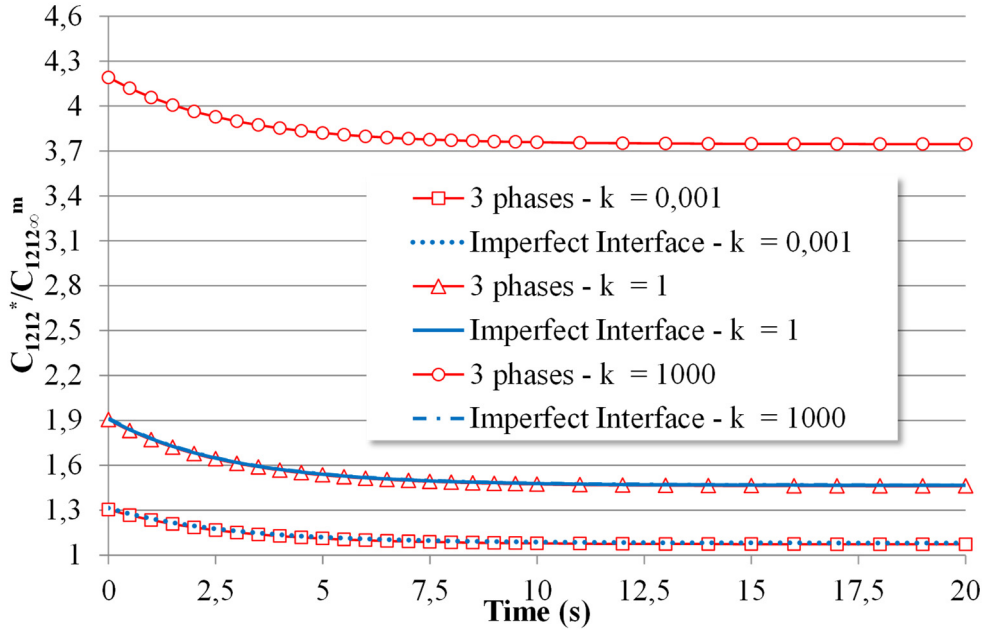

Figure 17: Homogenized relaxation function C_{1212}^{*} of the flat multilayer for different values of the ratio$k = G_i/G_m$.

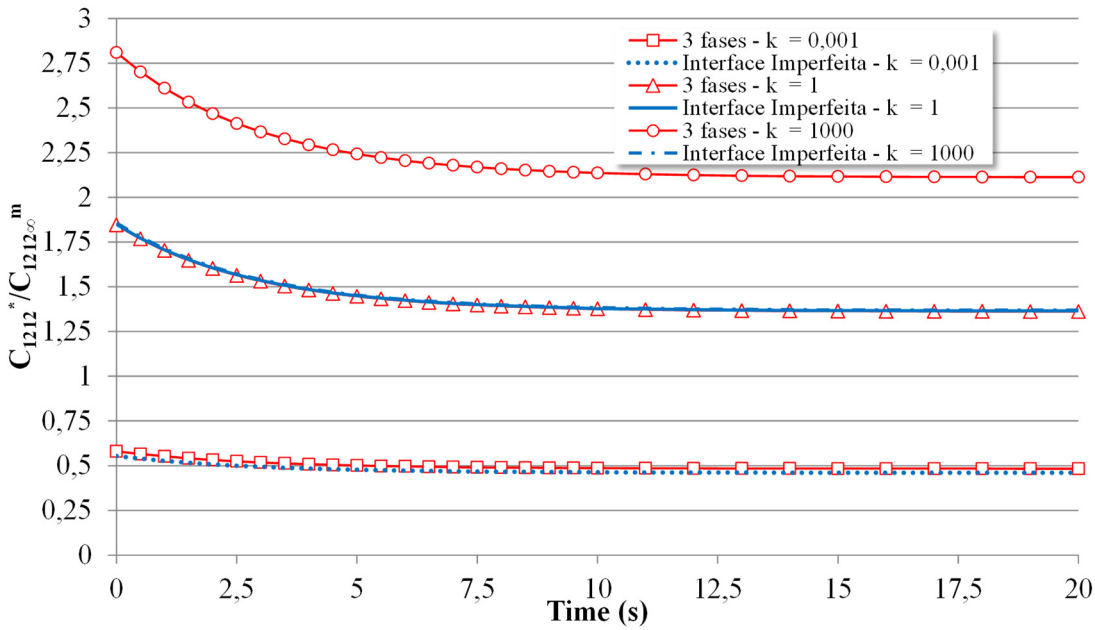

Figure 18: Homogenized relaxation function C_{1212}^{*} of the wavy multilayer for different values of the ratio$k = G_i/G_m$.

5 CONCLUSIONS

This paper presented a theoretical model for evaluation of the homogenized moduli of unidirectional periodic composite materials with linear viscoelastic phases, including flexible interphases between

the matrix and the fibers, based on the FVDAM theory. The model can be applied to materials composed of repeating unit cells with arbitrary internal architectural arrangements of fibers. To model the influence of the viscoelastic interphases, the paper presented an equivalent imperfect interface element derived under the hypothesis of continuity in tractions and discontinuity in displacements.

The proposed model operates directly in the time domain using a numerical incremental time-stepping procedure based on the concept of internal stress variables applicable to viscoelastic behavior described by generalized Maxwell models.

To demonstrate the performance of the presented formulation, the paper presented examples of homogenization for fiber reinforced composites and periodic multilayer materials with flat and wavy architectures. The efficiency of the imperfect interface element was verified through comparisons of computed homogenized viscoelastic moduli with analytical solutions and also with results obtained by the discretization of the repeating unit cell as constituted by three phases (matrix, reinforcement and interphase). Such comparisons showed a good performance of the proposed formulation.

Acknowledgments

The authors acknowledge the financial support provided by the Brazilian federal agencies CNPq and CAPES.

References

Bansal, Y., Pindera, M.-J., (2003). Efficient reformulation of the thermoelastic higher-order theory for FGMs. Journal of Thermal Stresses 26(11-12): 1055-1092.

Bathe, K.-J., (2014). Finite-element procedures in engineering analysis, Second edition, Klaus-Jürgen Bathe, Watertown.

Benveniste, Y., (2006). A general interface model for a three-dimensional curved thin anisotropic interphase between two anisotropic media. Journal of the Mechanics and Physics of Solids 54(4): 708-734.

Brinson, L.C., Lin, W.S., (1998). Comparison of micromechanics methods for effective properties of multiphase viscoelastic composites.Composite Structures 41: 353-367.

Cavalcante, M. A. A., Khatam, H., Pindera, M.-J., (2011). Homogenization of elastic–plastic periodic materials by FVDAM and FE approaches – an assessement. Composites: Part B 42: 1713–1730.

Cavalcante, M.A.A., Marques, S.P.C., (2014). Homogenization of periodic materials with viscoelastic phases using the generalized FVDAM theory. Computational Materials Science 87: 43-53.

Cavalcante, M.A.A., Marques, S.P.C., Pindera, M.-J., (2007). Parametric formulationof the finite-volume theory for functionally graded materials. Part I: Analysis. Journal of Applied Mechanics 74: 935–945.

Cavalcante, M.A.A., Pindera, M.-J., (2012). Generalized finite-volume theory for elastic stress analysis in solids mechanics - Part I: Framework. Journal of Applied Mechanics 79(5): 051006.

Cavalcante, M.A.A., Pindera, M.-J., (2014a). Generalized FVDAM theory for periodic materials undergoing finite deformations - Part I: Framework. Journal of Applied Mechanics 81: 021005-1.

Cavalcante, M.A.A., Pindera, M.-J., (2014b).Generalized FVDAM theory for periodic materials undergoing finite deformations - Part II: Results. Journal of Applied Mechanics 81: 021006-1.

Cavalcante, M.A.A., Pindera, M.-J., Khatam, H., (2012). Finite-volume micromechanics of periodic materials: past, present and future. Composites B 43(6): 2521-2543.

Christensen, R.M., (1969). Viscoelastic properties of heterogeneous media. Journal of the Mechanics and Physics of Solids 17: 23-41.

Debotton, G., Tevet-Deree, L., (2004).The response of a fiber-reinforced composite with a viscoelastic matrix phase. Journal of Composite Materials 38 (14): 1255-1277.

Doghri, I., Tinel, L., (2005). Micromechanical modeling and computation of elasto-plastic materials reinforced with distributed-orientation fibers. International Journal of Plasticity 21(10): 1919-1940.

Escarpini Filho, R. S., Marques, S.P.C., (2014). A Model for evaluation of effective thermal conductivity of periodic composites with poorly conducting interfaces. Materials Research 17(5): 1344-1355.

Eshelby, J.D., (1957). The determination of the elastic field of an ellipsoidal inclusion and related problems. Proceedings of the Royal Society of London 241: 376-396.

Friebel, C., Doghri, I., Legat,V., (2006). General mean-field homogenization schemes for viscoelastic composites containing multiple phases of coated inclusions. International Journal of Solids and Structures 43: 2513-2541.

Gattu, M., Khatam, H., Drago, A.S., Pindera, M.-J., (2008).Parametric finite-volume micromechanics of uniaxial continuously-reinforced periodic materials with elastic phases. J. Engineering Materials and Technology 130(3):031015.

Hashin, Z., (1962). The elastic moduli of heterogeneous materials. Journal of Applied Mechanics 29: 143-150.

Hashin, Z., (1965). Viscoelastic behavior of heterogeneous media. Journal of Applied Mechanics 32(3): 630-663.

Hashin, Z., (1970a). Complex moduli of viscoelastic composites—I. General theory and application to particulate composites. International Journal of Solids and Structures 6 (5): 539-552.

Hashin, Z., (1970b). Complex moduli of viscoelastic composites—II. Fiber reinforced materials. International Journal of Solids and Structures 6 (6): 797-807.

Hashin, Z., (1990). Thermoelastic properties of fiber composites with imperfect interface. Mechanics of Materials 8: 333-348.

Hashin, Z., (1991). Composite materials with viscoelastic interphase: creep and relaxation. Mechanics of Materials 11: 135–148.

Hashin, Z., (2002). Thin interphase/imperfect interface in elasticity with application to coated fibre composites. Journal of the Mechanics and Physics of Solids 50: 2509-2537.

Khatam, H., Pindera, M-J., (2009).Parametric finite-volume micromechanics of periodic materials with elastoplastic phases. International Journal of Plasticity 25(7):1386–411.

Laws, N., Mc Laughlin, R., (1978).Self-consistent estimates for the viscoelastic creep compliances of composite materials. Proceedings of the Royal Society of London. A.Mathematical and Physical Sciences 359: 251-273.

Luciano, R., Barbero, E.J., (1995). Analytical expressions for the relaxation moduli of linear viscoelastic composites with periodic microstructure. Journal of Applied Mechanics 62: 786-793.

Marques, S.P.C. and Creus, G.J., (2012).Computational Viscoelasticity, Springer-Verlag, Heidelberg.

Matzenmiller, A., Gerlach, S., (2004).Micromechanical modeling of viscoelastic composites with compliant fiber - matrix bonding. Computational Materials Science 29: 283-300.

Nemat-Nasser, S. and Hori, M., (1999). Micromechanics: Overall properties of heterogeneous materials, Second Edition, North-Holand, London.

Simo, J.C. and Hughes, T.J.R., (1998). Computational Inelasticity, Springer-Verlag New York, Inc.

Tran, A.B., Yvonnet, J., He, Q.-C., Toulemonde, C., Sanahuja, J., (2011). A simple computational homogenization method for structures made of linear heterogeneous viscoelastic materials. Computer Methods in Applied Mechanics and Engineering 200: 2956-2970.

Wang Y.M., Weng, G.J., (1992). The influence of inclusion shape on the overall viscoelastic behavior of composites. Journal of Applied Mechanics 59: 510-518.

Zaoui, A., (2002). Continuum Micromechanics: Survey. Journal of Engineering Mechanics 128(8): 808-816.

APPENDIX A

Matrices appearing in the subvolume derivation are given below.

$$\mathbf{D}_{in} = \mathbf{diag}[\boldsymbol{n}_{in}^{(1)} \quad \boldsymbol{n}_{in}^{(2)} \quad \boldsymbol{n}_{in}^{(3)} \quad \boldsymbol{n}_{in}^{(4)}], \qquad \mathbf{D}_{out} = \mathbf{diag}[\boldsymbol{n}_{out}^{(1)} \quad \boldsymbol{n}_{out}^{(2)} \quad \boldsymbol{n}_{out}^{(3)} \quad \boldsymbol{n}_{out}^{(4)}] \tag{A.1}$$

with $\mathrm{n}_{\mathrm{in}}^{(\mathrm{f})} = \begin{bmatrix} \mathrm{n}_2 & 0 & \mathrm{n}_3 \\ 0 & \mathrm{n}_3 & \mathrm{n}_2 \end{bmatrix}^{(\mathrm{f})}$ and $\mathrm{n}_{\mathrm{out}}^{(\mathrm{f})} = [\mathrm{n}_2 \quad \mathrm{n}_3]^{(\mathrm{f})}$. The symbol **diag** means diagonal matrix.

$$\mathbf{C}_{\mathrm{in}} = \mathbf{diag}[\mathbf{C}_{\mathrm{in}}^{\infty} \quad \mathbf{C}_{\mathrm{in}}^{\infty} \quad \mathbf{C}_{\mathrm{in}}^{\infty} \quad \mathbf{C}_{\mathrm{in}}^{\infty}], \qquad \mathbf{C}_{\mathrm{out}} = \mathbf{diag}[\mathbf{C}_{\mathrm{out}}^{\infty} \quad \mathbf{C}_{\mathrm{out}}^{\infty} \quad \mathbf{C}_{\mathrm{out}}^{\infty} \quad \mathbf{C}_{\mathrm{out}}^{\infty}] \tag{A.2}$$

where $\mathrm{C}_{\mathrm{in}}^{\infty}$ and $\mathrm{C}_{\mathrm{out}}^{\infty}$ are given in Eq. (40).

$$\widehat{\mathbf{H}}_{\mathrm{in}} = \left[\widehat{\mathbf{H}}_{\mathrm{in}}^{(1)} \quad \widehat{\mathbf{H}}_{\mathrm{in}}^{(2)} \quad \widehat{\mathbf{H}}_{\mathrm{in}}^{(3)} \quad \widehat{\mathbf{H}}_{\mathrm{in}}^{(4)}\right]^{\mathrm{T}}, \qquad \widehat{\mathbf{H}}_{\mathrm{out}} = \left[\widehat{\mathbf{H}}_{\mathrm{out}}^{(1)} \quad \widehat{\mathbf{H}}_{\mathrm{out}}^{(2)} \quad \widehat{\mathbf{H}}_{\mathrm{out}}^{(3)} \quad \widehat{\mathbf{H}}_{\mathrm{out}}^{(4)}\right]^{\mathrm{T}} \tag{A.3}$$

with $\widehat{\mathrm{H}}_{\mathrm{in}}^{(\mathrm{f})} = \begin{bmatrix} \widehat{\mathrm{H}}_{22} \\ \widehat{\mathrm{H}}_{33} \\ \widehat{\mathrm{H}}_{23} \end{bmatrix}^{(\mathrm{f})}$ and $\widehat{\mathrm{H}}_{\mathrm{out}}^{(\mathrm{f})} = \begin{bmatrix} \widehat{\mathrm{H}}_{12}(\mathrm{t}) \\ \widehat{\mathrm{H}}_{13}(\mathrm{t}) \end{bmatrix}^{(\mathrm{f})}$

$$\mathbf{N}_{in} = \left[\boldsymbol{n}_{in}^{(1)} \quad \boldsymbol{n}_{in}^{(2)} \quad \boldsymbol{n}_{in}^{(3)} \quad \boldsymbol{n}_{in}^{(4)}\right]^{\mathrm{T}}, \qquad \mathbf{N}_{out} = \left[\boldsymbol{n}_{out}^{(1)} \quad \boldsymbol{n}_{out}^{(2)} \quad \boldsymbol{n}_{out}^{(3)} \quad \boldsymbol{n}_{out}^{(4)}\right]^{\mathrm{T}} \tag{A.4}$$

$$\overline{\mathbf{A}}_{in} = \mathbf{D}_{in}\mathbf{C}_{in}\mathbf{E}_{in}\mathbf{B}_{in}\mathbf{A}_{in}, \qquad \overline{\mathbf{A}}_{out} = \mathbf{D}_{out}\mathbf{C}_{out}\mathbf{B}_{out}\mathbf{A}_{out} \tag{A.5}$$

where $\mathbf{E}_{in} = \mathbf{diag}[\bar{\mathbf{E}}\bar{\mathbf{E}}\ \bar{\mathbf{E}}\bar{\mathbf{E}}]$, $\mathbf{B}_{in} = \mathbf{diag}[\hat{\mathbf{J}}\hat{\mathbf{J}}\hat{\mathbf{J}}\hat{\mathbf{J}}\hat{\mathbf{J}}\hat{\mathbf{J}}\hat{\mathbf{J}}\hat{\mathbf{J}}]$, $\mathbf{B}_{out} = \mathbf{diag}[\hat{\mathbf{J}}\hat{\mathbf{J}}\hat{\mathbf{J}}\hat{\mathbf{J}}]$,

$$\mathrm{A}_{\mathrm{in}} = \begin{bmatrix} \mathrm{A}_4 & 0 & \mathrm{A}_1 & 0 & \mathrm{A}_3 & 0 & \mathrm{A}_2 & 0 \\ 0 & \mathrm{A}_4 & 0 & \mathrm{A}_1 & 0 & \mathrm{A}_3 & 0 & \mathrm{A}_2 \end{bmatrix}^{\mathrm{T}} \text{ and } \mathbf{A}_{out} = [\mathrm{A}_4 \quad \mathrm{A}_1 \quad \mathrm{A}_3 \quad \mathrm{A}_2]^{\mathrm{T}}$$

$$\boldsymbol{\Phi}_{\mathrm{in}} = \mathbf{L}_{\mathrm{in}}\overline{\mathbf{A}}_{\mathrm{in}}\overline{\mathbf{N}}_{\mathrm{in}}, \qquad \boldsymbol{\Phi}_{\mathrm{out}} = \mathbf{L}_{\mathrm{out}}\overline{\mathbf{A}}_{\mathrm{out}}\overline{\mathbf{N}}_{\mathrm{out}} \tag{A.6}$$

$$\boldsymbol{\omega}_{in} = \mathbf{L}_{in}\mathbf{N}_{in}\mathbf{C}_{in}^{\infty}, \qquad \boldsymbol{\omega}_{out} = \mathbf{L}_{out}\mathbf{N}_{out}\mathbf{C}_{out}^{\infty} \tag{A.7}$$

$$\boldsymbol{\theta}_{\mathrm{in}} = \mathbf{L}_{in}\overline{\mathbf{A}}_{in}\mathbf{P}_{in}, \qquad \boldsymbol{\theta}_{out} = \mathbf{L}_{out}\overline{\mathbf{A}}_{out}\mathbf{P}_{out} \tag{A.8}$$

with

$$\mathbf{L}_{in} = \begin{bmatrix} \mathrm{L}_1 & 0 & \mathrm{L}_2 & 0 & \mathrm{L}_3 & 0 & \mathrm{L}_4 & 0 \\ 0 & \mathrm{L}_1 & 0 & \mathrm{L}_2 & 0 & \mathrm{L}_3 & 0 & \mathrm{L}_4 \end{bmatrix}^{\mathrm{T}}, \qquad \mathbf{L}_{out} = [\mathrm{L}_1 \quad \mathrm{L}_2 \quad \mathrm{L}_3 \quad \mathrm{L}_4]$$

$$\overline{\mathbf{N}}_{in} = \begin{bmatrix} 0 & 0 & 1 & 1 & 0 & 0 & 0 & 0 \\ 0 & 0 & 0 & 0 & 0 & 0 & 1 & 1 \end{bmatrix}^{\mathrm{T}}, \qquad \overline{\mathbf{N}}_{out} = [0 \quad 0 \quad 1 \quad 1]^{\mathrm{T}}$$

$$\mathbf{P}_{in} = \begin{bmatrix} 0 & 0 & 1/2 & 0 & 0 & 0 & -1/2 & 0 \\ -1/2 & 0 & 0 & 0 & 1/2 & 0 & 0 & 0 \\ 0 & 0 & 1/2 & 0 & 0 & 0 & 1/2 & 0 \\ 1/2 & 0 & 0 & 0 & 1/2 & 0 & 0 & 0 \\ 0 & 0 & 0 & 1/2 & 0 & 0 & 0 & -1/2 \\ 0 & -1/2 & 0 & 0 & 0 & 1/2 & 0 & 0 \\ 0 & 0 & 0 & 1/2 & 0 & 0 & 0 & 1/2 \\ 0 & 1/2 & 0 & 0 & 0 & 1/2 & 0 & 0 \end{bmatrix}$$

$$\mathbf{P}_{out} = \begin{bmatrix} 0 & 1/2 & 0 & -1/2 \\ -1/2 & 0 & 1/2 & 0 \\ 0 & 1/2 & 0 & 1/2 \\ 1/2 & 0 & 1/2 & 0 \end{bmatrix}$$

$$\bar{\mathbf{B}}_{in} = \mathbf{P}_{in} - \bar{\mathbf{N}}_{in}\boldsymbol{\Phi}_{in}^{-1}\boldsymbol{\theta}_{in}, \qquad \bar{\mathbf{B}}_{out} = \mathbf{P}_{out} - \bar{\mathbf{N}}_{out}\boldsymbol{\Phi}_{out}^{-1}\boldsymbol{\theta}_{\mathrm{out}} \tag{A.9}$$

$$\mathbf{S}_{\mathrm{in}} = \mathbf{N}_{\mathrm{in}}\mathbf{C}_{\mathrm{in}}^{\infty} - \bar{\mathbf{A}}_{\mathrm{in}}\bar{\mathbf{N}}_{\mathrm{in}}\boldsymbol{\Phi}_{\mathrm{in}}^{-1}\boldsymbol{\omega}_{\mathrm{in}}, \qquad \mathbf{S}_{\mathrm{out}} = \mathbf{N}_{\mathrm{out}}\mathbf{C}_{\mathrm{out}}^{\infty} - \bar{\mathbf{A}}_{\mathrm{out}}\bar{\mathbf{N}}_{\mathrm{out}}\boldsymbol{\Phi}_{\mathrm{out}}^{-1}\boldsymbol{\omega}_{\mathrm{out}} \tag{A.10}$$

$$\mathbf{F}_{\mathrm{in}} = \mathbf{D}_{\mathrm{in}} - \bar{\mathbf{A}}_{\mathrm{in}}\bar{\mathbf{N}}_{\mathrm{in}}\boldsymbol{\Phi}_{\mathrm{in}}^{-1}\mathbf{L}_{\mathrm{in}}\mathbf{D}_{\mathrm{in}}, \qquad \mathbf{F}_{\mathrm{out}} = \mathbf{D}_{\mathrm{out}} - \bar{\mathbf{A}}_{\mathrm{out}}\bar{\mathbf{N}}_{\mathrm{out}}\boldsymbol{\Phi}_{\mathrm{out}}^{-1}\mathbf{L}_{\mathrm{out}}\mathbf{D}_{\mathrm{out}} \tag{A.11}$$

APPENDIX B

Matrices appearing in the imperfect interface element derivation are given below.

$$\mathbf{M} = \left[\sum_{j=1}^{N} \exp\left(-\frac{\Delta t}{\tau_{1j}}\right)\hat{q}_{1j} \sum_{j=1}^{N} \exp\left(-\frac{\Delta t}{\tau_{2j}}\right)\hat{q}_{2j} \sum_{j=1}^{N} \exp\left(-\frac{\Delta t}{\tau_{3j}}\right)\hat{q}_{3j}\right]^{\mathrm{T}} \tag{B.1}$$

$$\mathbf{Q} = \begin{bmatrix} -Q_1 & 0 & 0 & Q_1 & 0 & 0 \\ 0 & -Q_2 & 0 & 0 & Q & 0 \\ 0 & 0 & -Q_3 & 0 & 0 & Q_3 \end{bmatrix} \tag{B.2}$$

$$\mathbf{R} = \begin{bmatrix} -R_1 & 0 & 0 & R_1 & 0 & 0 \\ 0 & -R_2 & 0 & 0 & R_2 & 0 \\ 0 & 0 & -R_3 & 0 & 0 & R_3 \end{bmatrix} \tag{B.3}$$

$$\mathbf{K}_I = \begin{bmatrix} -K_1 & 0 & 0 & K_1 & 0 & 0 \\ 0 & -K_2 & 0 & 0 & K_2 & 0 \\ 0 & 0 & -K_3 & 0 & 0 & K_3 \end{bmatrix} \tag{B.4}$$

where the components $\mathrm{Q_i}$, $\mathrm{R_i}$ and $\mathrm{K_i}$ are defined in Eq. (55).